



Dynamic crushing of wood-based sandwich composite tubes

Romain Guélou, Florent Eyma, Arthur Cantarel, Samuel Rivallant, Bruno Castanié

► To cite this version:

Romain Guélou, Florent Eyma, Arthur Cantarel, Samuel Rivallant, Bruno Castanié. Dynamic crushing of wood-based sandwich composite tubes. *Mechanics of Advanced Materials and Structures*, 2021, pp.1-21. 10.1080/15376494.2021.1991533 . hal-03407710

HAL Id: hal-03407710

<https://hal.science/hal-03407710>

Submitted on 28 Oct 2021

HAL is a multi-disciplinary open access archive for the deposit and dissemination of scientific research documents, whether they are published or not. The documents may come from teaching and research institutions in France or abroad, or from public or private research centers.

L'archive ouverte pluridisciplinaire **HAL**, est destinée au dépôt et à la diffusion de documents scientifiques de niveau recherche, publiés ou non, émanant des établissements d'enseignement et de recherche français ou étrangers, des laboratoires publics ou privés.

Dynamic crushing of wood based sandwich composite tubes

R. Guélou^a, F. Eyma^a, A. Cantarel^a, S. Rivallant^a, B. Castanié^{a,*}

^aInstitut Clément Ader (ICA), ISAE, CNRS UMR 5312-INSA-Mines Albi-UPS, Toulouse, France

* Corresponding author: bruno.castanie@insa-toulouse.fr

Keywords: Wood veneers, Poplar, Composites, Sandwich, Crushing, Energy absorption, Tube, Dynamic

Abstract: The paper presents the results of dynamic crushing of sandwich tubes that had skins made of carbon or glass fibres - with epoxy resin - and an I214 poplar ply core. By increasing the number of poplar plies from two to six, the absorbed energy is doubled, showing the significant contribution of the wood. The Specific Energy Absorption of sandwiches with carbon fibre skins oscillated between 49.4 and 60 J/g while that with glass fibre skins varied from 35.4 to 43.3 J/g.

1. Introduction

Wood is a material that is respectful of the environment because it is renewable and requires little embodied energy (energy corresponding to the transformation of the raw product into the finished product) due to its ability to store carbon [1,2]. Wood is considered to be a credible substitute material for meeting sustainable development targets, particularly in the field of transport [3]. It is a material that has been used for many years in both civil engineering and aeronautics, where planes were made of wood until World War II and showed remarkable levels of performance [4]. Several French companies are showing renewed interest by either pursuing wood construction (Robin Aircraft [5]) with the DR401 (2700 units since 1972) or introducing it into their most recent structures ([6,7]). Studies have also shown that this material is particularly interesting for automobiles [8,9]. This renewal of interest is also shared by the academic world and recent studies demonstrate the interest of wood alone or in combination with natural fibres or modern materials such as glass, Kevlar, carbon or even aluminium, in particular in sandwich form [10-16]. An increasing number of recent academic studies have also shown

that wood has very good mechanical characteristics at low speed-low energy impact [17-23] and in compression after impact, with behaviour that is sometimes surprising compared to that of composites. The knockdown factor can reach 70 % for classical carbon Nomex sandwich and is less than 10% in certain configurations with plywood cores [24-26]. Historically, wood has also been identified as a material with good dynamic and crash absorption characteristics and has been used for a very long time, for example, in the transport of radioactive materials [27–28].

In previous papers, the authors looked into the crash behaviour of tubes laminated with plies in poplar alone I214 [29] and were able to show that this wood, one of the cheapest and lightest, had good SEA up to 30 J / kg for a material 40 times less expensive than CFRP, and renewable. As with composite tubes, exterior polar plies oriented at 90° and creating a “hoop effect” increased resistance to the crushing force, thus improving the SEA. It is therefore clear that sandwich tubes with a core in I214 poplar plies and the interior and exterior skins of the tube in carbon and fibreglass fabrics should be the next step. These configurations have been tested under quasi-static loads in [30].

It was shown that better energy absorption was obtained with all the poplar veneers at 0° because the “hoop effect” ensured by the outer and inner composite layers was sufficient. The average SEA of tubes with carbon skins was 61.2 J/g and remains quite constant, for an SEA gain of around 47% with respect to the sum of the two materials crushed independently. An average SEA of 32.5 J/g was obtained for tubes with glass skins. Coupling I214 poplar veneers with glass fibres allowed, in particular, a gain of 20% on absorbed energy and 22% on the SEA.

This paper is the continuation of [30] and presents the dynamic crushing of sandwich tubes with composite skins in carbon or glass fibres and a core in I214 poplar veneers. The objective is to understand the behaviour of these structures from the point of view of dynamics.

2. Materials, test specimens and setup

2.1. Materials and manufacturing

The sandwich tubes were manufactured using a metal mandrel, on which the two inner composite layers (carbon or glass fabrics) were stacked first. It was presented in [30] and is briefly recalled here. The 1 mm thick I214 poplar veneers, supplied by the Garnica company, were then wound up. A heat-shrinkable tape was wound around them to provide pressure during crosslinking. After this first curing cycle, the 2 outer composite plies (carbon or glass fabrics) were finally stacked and a second curing cycle was performed with a wound heat-shrink band.

The monolithic carbon or glass tubes were manufactured in the same way: four composite plies were stacked over the metal mandrel and a heat-shrinkable strip was wound around them. The curing cycles were as follows:

- For carbon, 30 min at 90 °C then 2 h 20 min at 120 °C,
- For glass, 30 min at 90 °C then 1 hour at 120 °C.

The prepregs used were supplied by Hexcel: the carbon plies were made with the prepreg M79/42%/200T2/ CHR-3K and the glass plies were in prepreg M9.6GF/42%/200T2/G, inducing theoretical fibre volume fractions of 44% and 39% respectively. These two prepregs were 2-2 twills having an areal weight of 345 g/m² and were oriented at [0/90] to obtain a hoop effect.

The wood glue used to pre-glue the veneers before they were rolled up was Kleiberit PUR 510 FIBERBOND glue, a one-component polyurethane-based glue that hardens by reaction with humidity, with a basis weight of 250 g/m². When the I214 poplar veneers had been stacked around the mandrel, the bonding was carried out with a relative humidity of between 8.8 and 9.8%. The density of the I214 veneers was 0.368 g/cm³.

The inner diameter of the tubes was 50 mm and their final length was 120 mm. A 45° chamfer was made around the entire thickness of the tubes (Fig. 1) in order to lower the peak load and control the side of failure initiation.

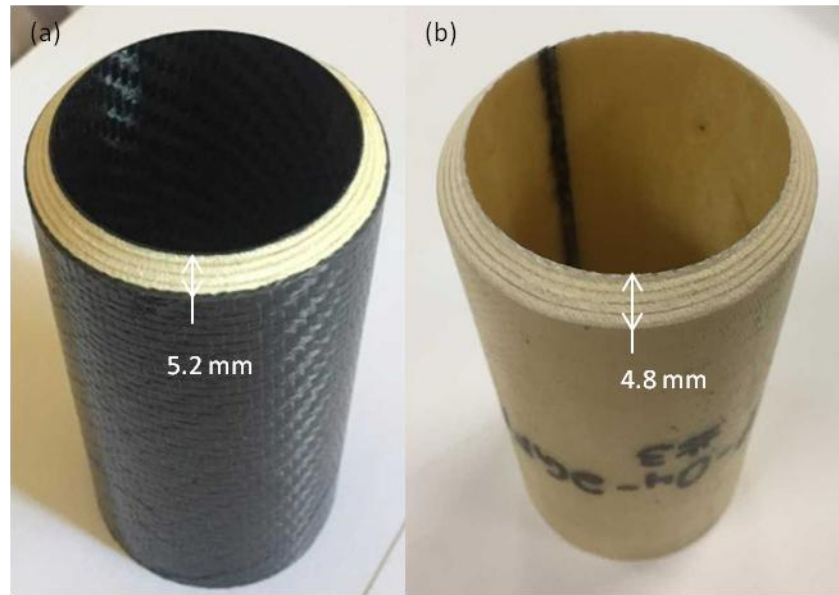


Fig. 1: Pristine sandwich tubes, (a) [2CFRP-[0₄]-2CFRP]-#3, (b) [2CFRP-[0₄]-2CFRP]-#3

The effect of wood was studied by varying the number of I214 plies from two to six while keeping a constant number of interior and exterior composite plies (carbon or glass). A sandwich tube had two interior composite plies and two exterior plies that thus constituted the skins. The composite tubes alone, intended for the evaluation of the coupling effects, then had four 4 plies in total. The sandwich tubes were defined by the following notation: [2GFRP- [0_n]-2GFRP] describing two glass plies on the inside and two plies on the outside, and n poplar plies oriented at 0° (0° being the longitudinal axis of the tube). The composite tubes were then defined by the notation [GFRP] or [CFRP] depending on the nature of the fibres. They always had four plies in total.

	Dynamic		Dynamic
[2CFRP-[0 ₆]-2CFRP]	3	[2GFRP-[0 ₆]-2GFRP]	3
[2CFRP-[0 ₅]-2CFRP]	3	[2GFRP-[0 ₅]-2GFRP]	3
[2CFRP-[0 ₄]-2CFRP]	3	[2GFRP-[0 ₄]-2GFRP]	3
[2CFRP-[0 ₃]-2CFRP]	3	[2GFRP-[0 ₃]-2GFRP]	3
[2CFRP-[0 ₂]-2CFRP]	3	[2GFRP-[0 ₂]-2GFRP]	3
[CFRP]	3	[GFRP]	3
[90/0 ₄ /90] (already crushed in [29])	3		
Total number of tubes	39		

Tab. 1: Summary of the test matrix

The poplar veneers were characterized mechanically in [30] by carrying out six tensile tests on a specimen of two l214 plies glued together in the transverse and longitudinal directions (same wood glue and same areal density).

2.2. Dynamic setup

As in [29], the dynamic tests were performed using a drop weight tower (Fig. 2). The initial crushing speeds were between 8.4 and 8.8 m / s. The device was equipped with a ballast mass (81 or 114 kg depending on the number of poplar plies). The mass of ballast was sufficient to provide more energy than that absorbed by the tube, so as to obtain an almost constant crushing speed. The excess energy was collected by a stop system that transferred this excess to honeycombs located below the lower plate. The stops allowed approximately 85-90 mm to be crushed and enabled observation of the tubes after crushing. A 100 kN force sensor was located between the (upper) crushing plate and the masses so that the force during the crushing could be acquired at a frequency of 1 MHz. A method of double integration from the effort and the initial speed gave the displacement. The movement was also verified by means of images from high speed cameras that were synchronized with the force sensor.

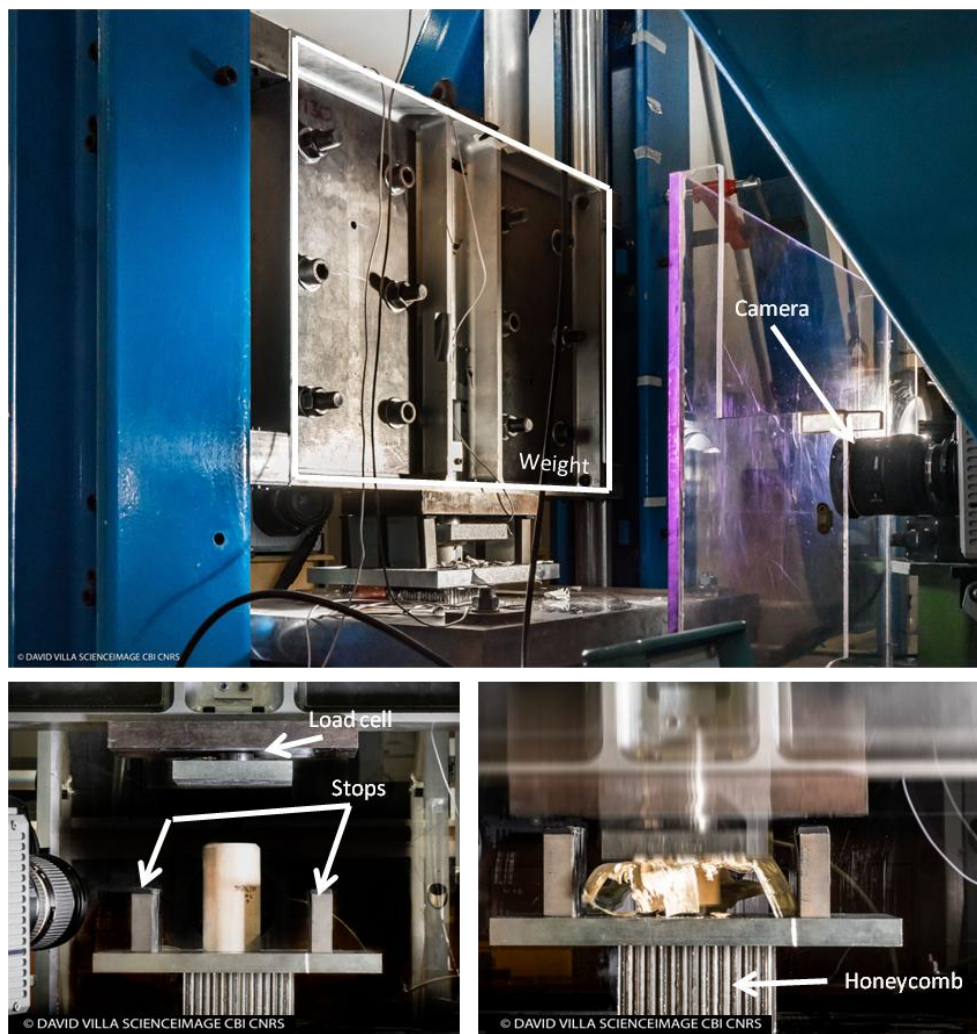


Fig. 2: Drop tower test device for dynamic crushing

From the force-displacement curve obtained during the crush, several quantities and performance criteria were extracted. The peak effort is noted F_{\max} . The average effort in the plateau is called F_{plateau} . The CFE (Crush Force Efficiency) is the ratio between the average effort and the maximum effort ($F_{\text{plateau}}/F_{\max}$).

In general, when designing a shock absorber, a CFE very close to 1 is desirable, to limit the forces in the rest of the structure during a crash. The energy absorbed here was calculated only on the first 80 mm crushed and is noted $EA_{\text{tot}_80\text{mm}}$. It was thus possible to compare static and dynamic crushing even though the dynamic crushing lengths varied somewhat. Finally the SEA was also defined on the first 80 millimetres crushed and was therefore calculated as follows: $SEA_{\text{tot}_80\text{mm}} = \frac{F_{\text{tot}_80\text{mm}}}{\rho \times S}$ (J/g), with ρ the average density of the tube (prepreg + glue + veneers) and S the section.

3. Results and discussion

3.1. Sandwich tubes with carbon skins

The average crushing speed obtained from the falling weight tests was 8.8 m/s. The dynamic crushing curves are shown in Fig. 3.

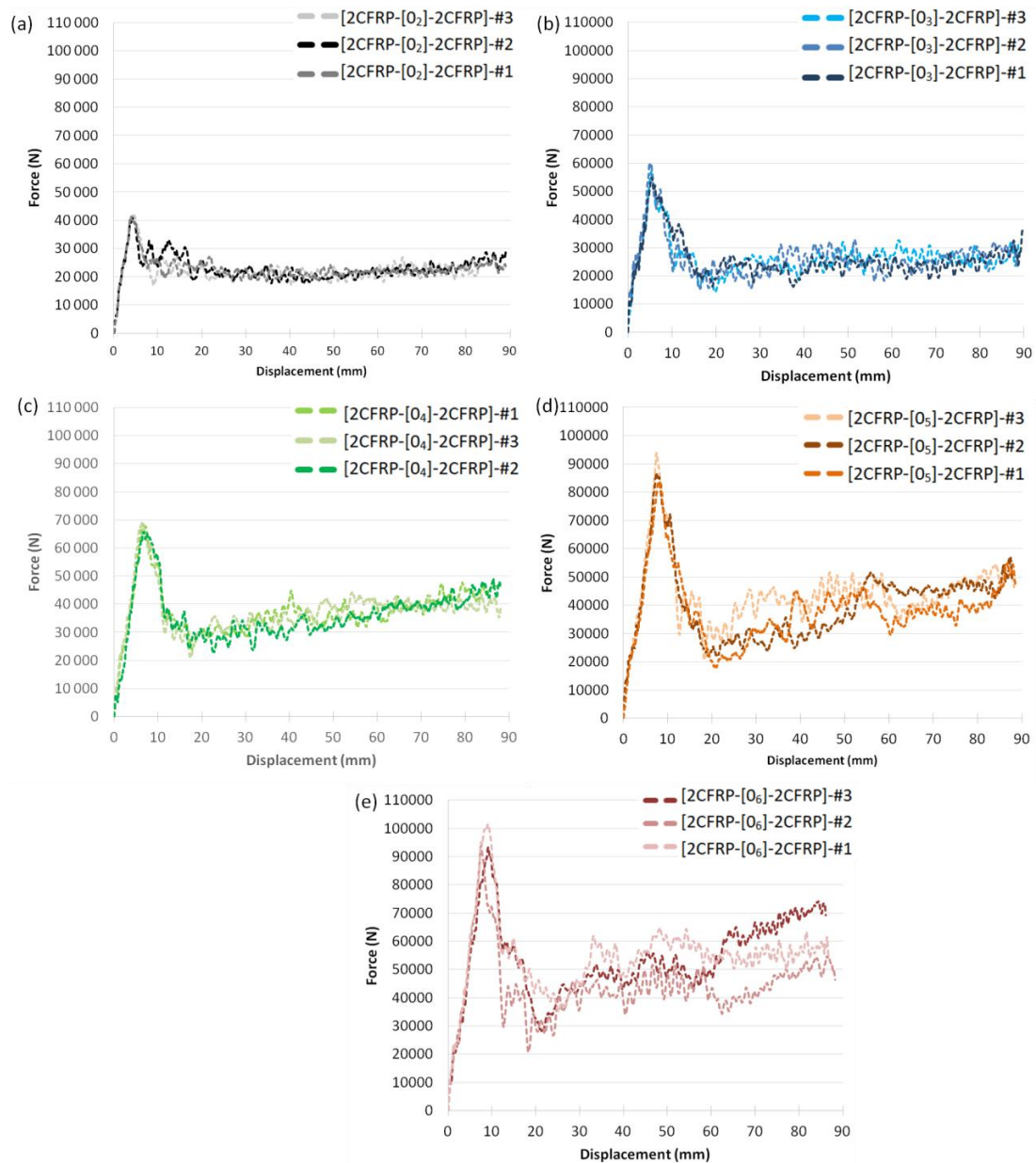


Fig. 3: Dynamic force-displacement curves of tubes (a) [2CFRP-[0₂]-2CFRP] (b) [2CFRP-[0₃]-2CFRP] (c) [2CFRP-[0₄]-2CFRP] (d) [2CFRP-[0₅]-2CFRP] (e) [2CFRP-[0₆]-2CFRP]

The typical phases are visible: initiation, transition and plateau. For tubes with four, five or six l214 plies, the plateau rises as the crushing advances. As the internal compaction of the debris occurs over the same internal diameter, the more the number of l214 plies increases, the more the compaction participates in crushing (Fig. 6). The dynamic performances are presented in Tab. 2.

	Mass g	Thickness mm	F _{max} N	L _{plateau} mm	F _{plateau} N	CFE	EA _{tot_80mm} J	SEA _{tot_80mm} J/g
[2CFRP-[0 ₂]-2CFRP] - #1	49.0	2.93	41 389	81.4	20 440	0.49	1 718	54.3
[2CFRP-[0 ₂]-2CFRP] - #2	49.2	2.98	40 825	82.6	22 723	0.56	1 807	54.4
[2CFRP-[0 ₂]-2CFRP] - #3	49.1	2.92	42 067	80.4	21 782	0.52	1 777	53.6

Average	49.1	2.94	41 427	81.5	21 649	0.52	1 767	54.1
Standard deviation	0.1	0.03	622	1.1	1 147	0.03	45	0.5
[2CFRP-[0 ₃]-2CFRP] - #1	61.8	4.34	54 968	74.3	23 739	0.43	2 020	48.1
[2CFRP-[0 ₃]-2CFRP] - #2	61.8	4.35	60 158	78.6	24 871	0.41	2 079	49.4
[2CFRP-[0 ₃]-2CFRP] - #3	61.1	4.27	57 269	78.4	25 153	0.44	2 110	50.8
Average	61.6	4.32	57 465	77.1	24 588	0.43	2 070	49.4
Standard deviation	0.4	0.04	2 601	2.4	749	0.01	46	1.3
[2CFRP-[0 ₄]-2CFRP] - #1	75.7	5.20	68 481	75.7	36 682	0.54	2 948	57.1
[2CFRP-[0 ₄]-2CFRP] - #2	75.1	5.23	65 819	76.3	35 040	0.53	2 812	54.8
[2CFRP-[0 ₄]-2CFRP] - #3	75.2	5.19	69 228	77.2	36 140	0.52	2 983	58.1
Average	75.3	5.21	67 843	76.4	35 954	0.53	2 915	56.7
Standard deviation	0.3	0.02	1 792	0.7	837	0.01	90	1.7
[2CFRP-[0 ₅]-2CFRP] - #1	91.8	6.37	93 836	75.5	42 392	0.45	3 457	54.8
[2CFRP-[0 ₅]-2CFRP] - #2	90.9	6.50	86 722	74.6	37 819	0.44	3 132	50.1
[2CFRP-[0 ₅]-2CFRP] - #3	88.9	6.44	83 816	73.4	36 083	0.43	2 996	49.0
Average	90.5	6.44	88 125	74.5	38 765	0.44	3 195	51.3
Standard deviation	1.5	0.07	5 155	1.1	3 259	0.01	237	3.1
[2CFRP-[0 ₆]-2CFRP] - #1	102.0	7.51	101 383	74.3	53 462	0.53	4 342	61.5
[2CFRP-[0 ₆]-2CFRP] - #2	101.9	7.50	100 587	71.8	50 729	0.50	4 178	59.3
[2CFRP-[0 ₆]-2CFRP] - #3	102.3	7.65	93 427	73.6	53 184	0.57	4 185	59.2
Average	102.1	7.52	98 466	73.2	52 459	0.53	4 235	60.0
Standard deviation	0.2	0.03	4 382	1.3	1 504	0.03	93	1.3

Tab. 2: Results for dynamic crushing of [2CFRP-[0_n]-2CFRP]_{2≤n≤6}

The failure mode of this configuration is initiated by the flattening of the chamfer in contact with the crushing plate. The outer and inner skins then come into contact with the platter and are then forced to splay inwards and outwards. The deformation imposed on the fibres oriented at 90° causes them to break and allows the tube to dissociate into bundles. As the crushing continues, the bundles and splaying of the inner and outer skins create petals (Fig. 4).

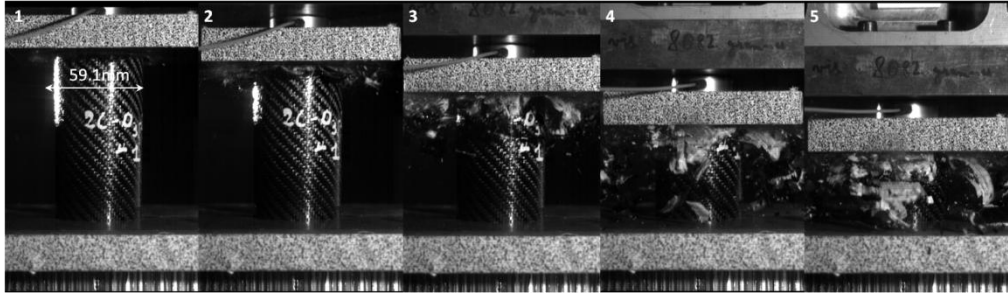
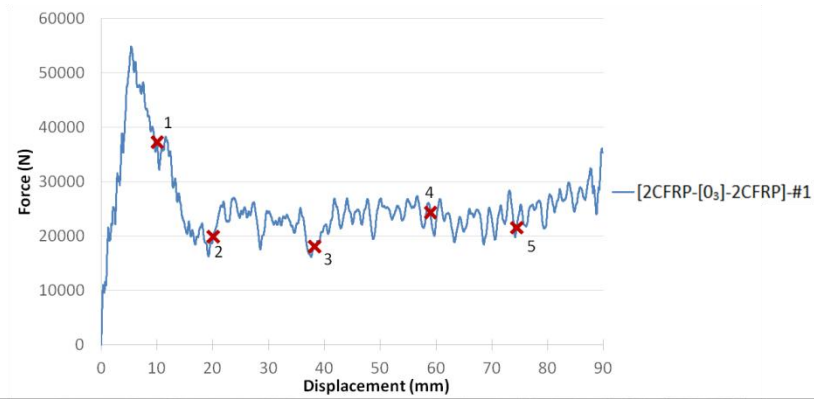


Fig. 4: Dynamic failure of tube [2CFRP-[0₃]-2CFRP]-#1 and association of pictures and points on the force displacement curve.

Post-crash analysis of the tubes shows fairly significant debris compaction within the tube (Fig. 5).

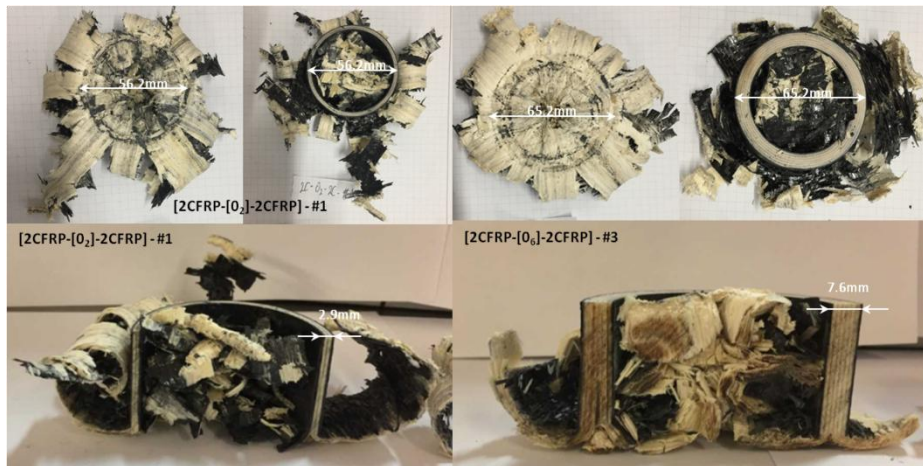


Fig. 5: Dynamic destruction of tubes [2CFRP-[0₂]-2CFRP]-#1 and [2CFRP-[0₆]-2CFRP]-#3 and of ½ tubes [2CFRP-[0₃]-2CFRP]-#3 and [2CFRP-[0₄]-2CFRP]-#1

The tubes have a generally similar failure mode but it is difficult to establish a link between the performance drops of configurations with different numbers of I214 plies and the differences in failure modes: the same configuration can present different failure patterns (Fig. 6), a common item for issue in crash testing.

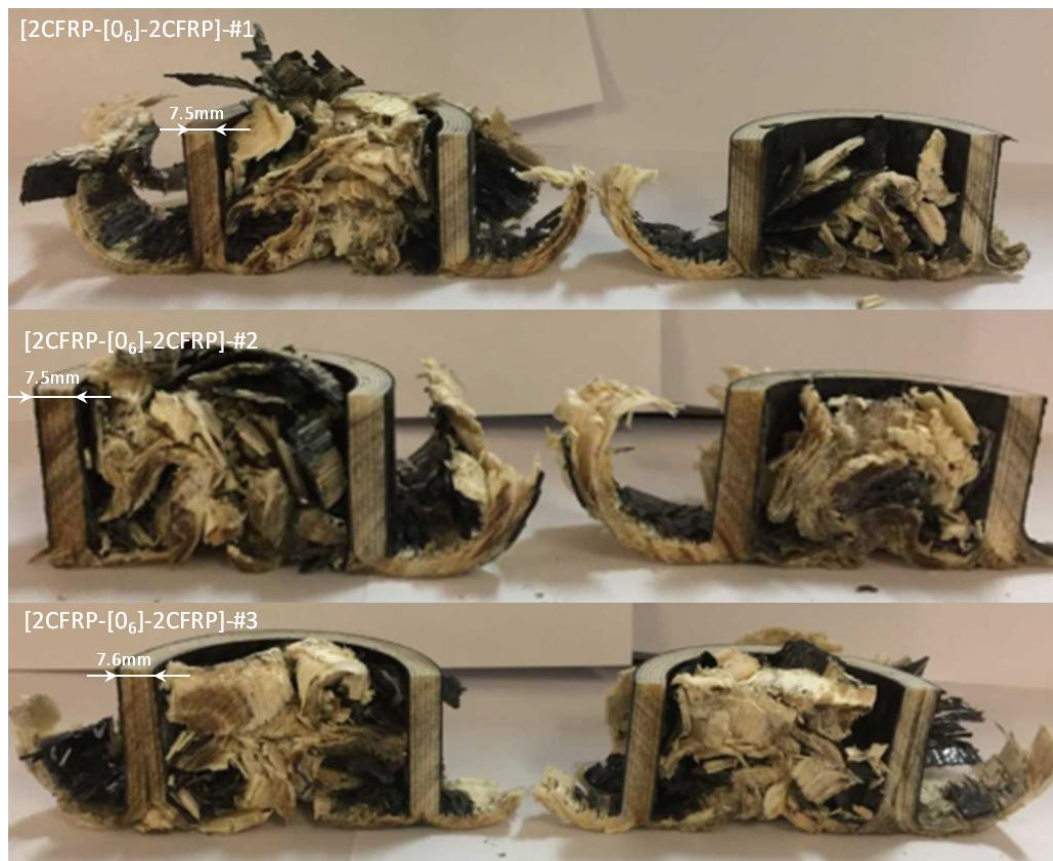


Fig. 6: Post-crush patterns of half sandwich tubes [2CFRP-[0₆]-2CFRP].

Here, for the [2CFRP-[0₆]-2CFRP] configuration, which shows good repeatability (Tab. 2) between these tubes, the failure mode is generally similar but there are differences, e.g. different central cracking position. Moreover, on the same tube, it can be seen that the failure front changes between the two half-tubes: [2CFRP- [0₆]-2CFRP] # 2, for example, exhibits one wall with bending over its entire thickness while the other wall is divided into two inner and outer parts an inner and an outer part.

Absorbed energy and SEA are plotted versus the number of folds in Fig. 7 (a). As splaying and internal debris compaction constitute the overall ruin mechanism of each ply configuration, the peak load and mean crush force at the plateau are plotted as a function of the section of the tubes in Fig. 7. (b).

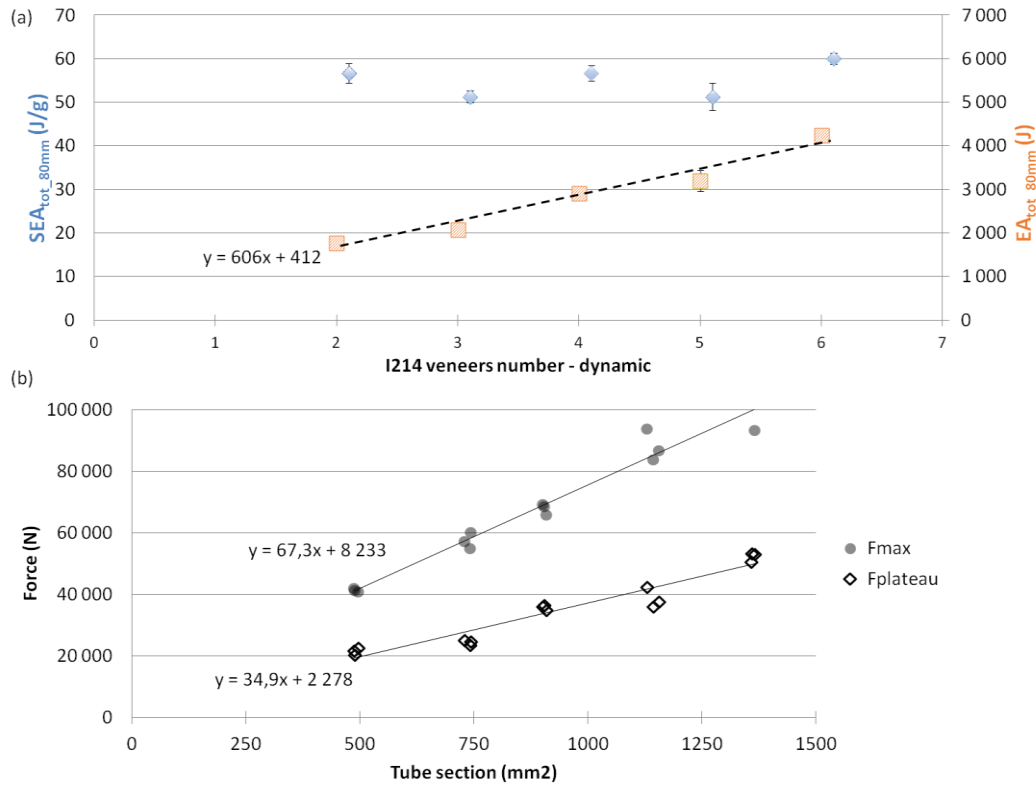


Fig. 7: (a) Evolution of EA_{tot_80mm} and SEA_{tot_80mm} versus the number of I214 layers. (b) Maximum and plateau force versus tube sections for tubes with carbon skins.

The energy absorbed increases linearly with the number of I214 folds, as expressed by the equation $EA_{tot_80mm} = 606 \times \text{number of layers}_{I214} + 412$, with 606 J which would represent the contribution of a single I214 poplar layer and 412 J the contribution of carbon skins. On average, the SEA oscillates between 48.1 J / g for the lowest value ([2CFRP-[0₃]-2CFRP]) and 61.5 J/g ([2CFRP-[0₆]-2CFRP]).

The peak load and the mean crushing force increases linearly with the section. The load peaks are higher than the average forces, the difference depending on the section of the tubes **OK?**. This is due to a more efficient failure mechanism during the loading phase than during the plateau phase. The equation of these two quantities confirms that the carbon fibre skins and the I214 plies work more efficiently in the loading phase than in the plateau phase: 67.3 MPa for the I214 layers and 8 233 N for the carbon skins versus 34.9 MPa and 2278 N respectively. The average crush stress of an I214 ply corresponds to overall failure mechanisms such as splaying and internal debris compaction and is 34.9 MPa.

3.2. Sandwich tubes with glass skins

The average crushing speed obtained from the falling weight tests was 8.4 m/s. The dynamic crushing curves are shown in Fig. 8.

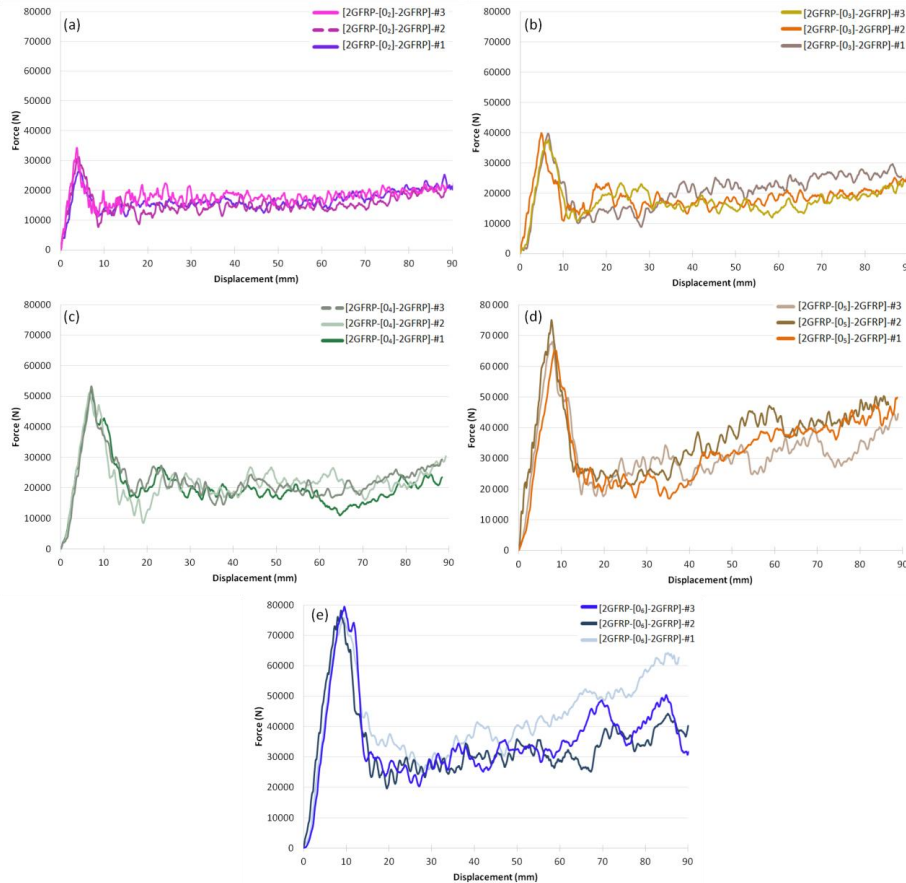


Fig. 8: Dynamic force-displacement curves for tubes (a) [2GFRP-[0₂]-2GFRP] (b) [2GFRP-[0₃]-2GFRP] (c) [2GFRP-[0₄]-2GFRP] (d) [2GFRP-[0₅]-2GFRP] (e) [2GFRP-[0₆]-2GFRP]

Again, the three phases (initiation, transition and plateau) are found. As with the sandwich tubes with carbon skins, for five and six layers of poplar, the crushing force is no longer constant and rises in the plateau phase as the crushing increases. The compaction of the interior debris may be responsible for this rise. The peak load, the plateau force and, therefore, the energy absorbed increase with the number of 1214 layers, (Tab. 3).

	g	mm	N	mm	N	/	J	J/g
	Mass	Thickness	F _{max}	L _{plateau}	F _{plateau}	CFE	EA _{tot_80mm}	SEA _{plateau}
[2GFRP-[0 ₂]-2GFRP] - #1	46.5	2.86	26 574	82.0	16 725	0.63	1 284	42.8
[2GFRP-[0 ₂]-2GFRP] - #2	47.9	2.99	31 163	82.3	14 695	0.47	1 203	36.5

[2GFRP-[0 ₂]-2GFRP] - #3	48.0	2.90	34 353	82.3	17 956	0.52	1 428	44.4
Average	47.5	2.92	30 697	82.2	16 459	0.54	1 305	41.2
Standard deviation	0.8	0.07	3 910	0.2	1 647	0.08	114	4.2
[2GFRP-[0 ₃]-2GFRP] - #1	58.4	4.25	39 771	75.0	20 827	0.53	1 612	40.8
[2GFRP-[0 ₃]-2GFRP] - #2	58.1	3.98	39 910	79.7	18 221	0.46	1 462	37.2
[2GFRP-[0 ₃]-2GFRP] - #3	59.6	4.11	37 706	77.7	17 228	0.46	1 388	34.4
Average	58.7	4.11	39 129	77.5	18 759	0.48	1 487	37.5
Standard deviation	0.8	0.14	1 234	2.4	1 859	0.04	114	3.2
[2GFRP-[0 ₄]-2GFRP] - #1	71.6	5.22	52 201	72.2	18 713	0.36	1 647	33.8
[2GFRP-[0 ₄]-2GFRP] - #2	71.6	5.11	51 071	75.9	21 046	0.41	1 760	36.1
[2GFRP-[0 ₄]-2GFRP] - #3	71.9	5.05	53 294	72.1	21 229	0.40	1 774	36.3
Average	71.7	5.13	52 189	73.4	20 329	0.39	1 727	35.4
Standard deviation	0.2	0.09	1 112	2.1	1 403	0.03	70	1.4
[2GFRP-[0 ₅]-2GFRP] - #1	85.2	6.09	65 266	74.8	31 963	0.49	2 512	41.8
[2GFRP-[0 ₅]-2GFRP] - #2	90.2	6.32	75 043	73.8	35 359	0.47	2 856	46.2
[2GFRP-[0 ₅]-2GFRP] - #3	87.9	6.28	68 083	74.4	29 835	0.44	2 448	42.1
Average	87.8	6.23	69 464	74.3	32 386	0.47	2 605	43.3
Standard deviation	2.5	0.12	5 032	0.5	2 786	0.03	220	2.5
[2GFRP-[0 ₆]-2GFRP] - #1	104.3	7.54	75 750	74.7	42 479	0.56	3 291	45.8
[2GFRP-[0 ₆]-2GFRP] - #2	102.5	7.24	78 173	74.3	31 219	0.40	2 648	37.6
[2GFRP-[0 ₆]-2GFRP] - #3	104.4	7.38	79 540	75.9	33 778	0.42	2 787	38.8
Average	103.7	7.39	77 821	75.0	35 825	0.46	2 908	40.7
Standard deviation	1.1	0.15	1 920	0.8	5 902	0.09	338	4.4

Tab. 3: Results for dynamic crushing of [2GFRP-[0_n]-2GFRP]_{2≤n≤6}

The failure mode is rather similar to that of the tubes with carbon fibre skins. In fact, in contact with the crushing plate, the chamfer flattens out, introducing enough deformation of the glass fibres oriented at 90° to force them to break. By breaking, they dissociate the tube into bundles and allow a splaying of the inner and outer skins as well as the I214 layers (Fig. 9).

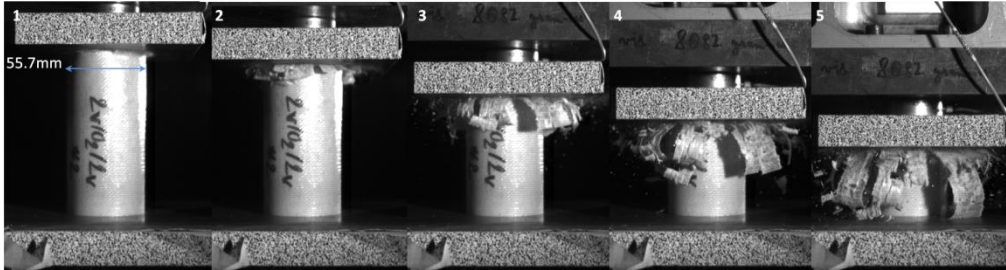
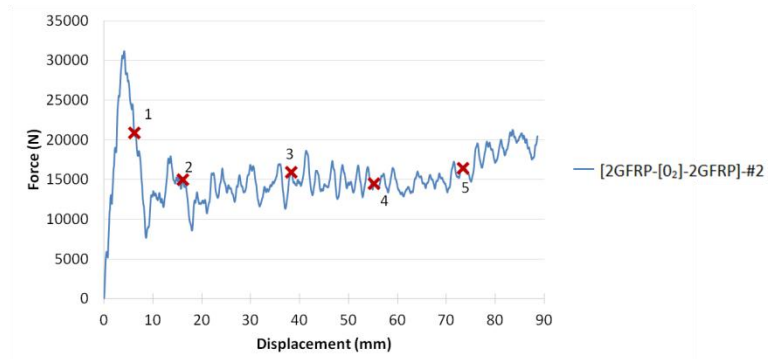


Fig. 9: Dynamic failure of tube [2GFRP-[0₂]-2GFRP]-#2 and association of pictures and points on the force/displacement curve.

The dissociation into bundles of the tube, accompanied by the splaying, leads to the formation of petals.

Fairly significant compaction was observed inside the tube (Fig. 10).

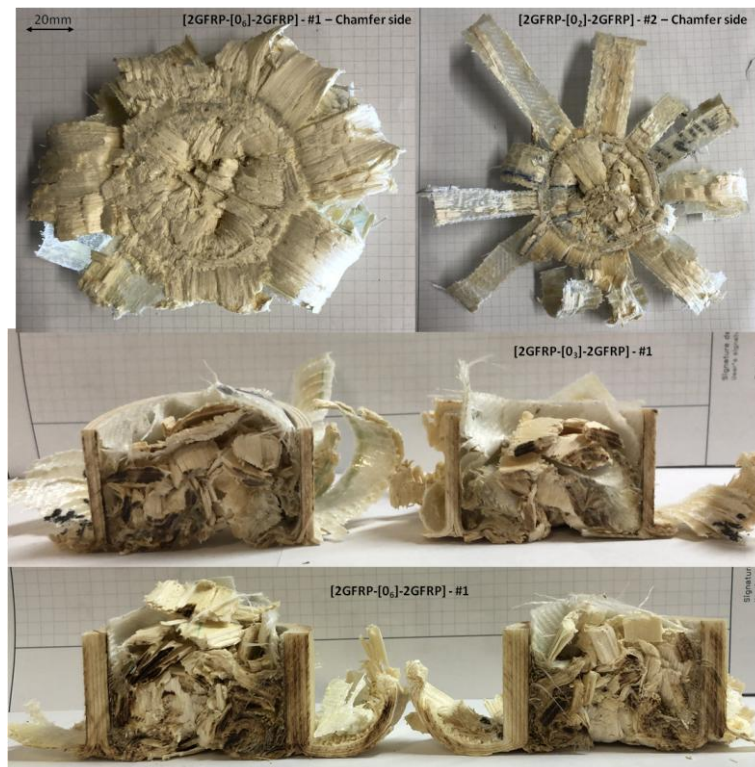


Fig. 10: Dynamic failure of tubes [2GFRP-[0₂]-2GFRP]-#1 and [2GFRP-[0₆]-2GFRP]-#1, and ½ tubes [2GFRP-[0₃]-2GFRP]-#1 and [2GFRP-[0₆]-2GFRP]-#1.

A slight debonding of the inner and outer skin and the I214 layers was also observed. Although the

energy absorbed varied almost linearly with the number of I214 plies used, SEA was not constant (Fig.

11 (a)). As the failure mechanisms were similar between the I214 ply configurations, the peak effort and the mean effort at the plateau level were plotted versus the section of the tubes (Fig. 11 (b)).

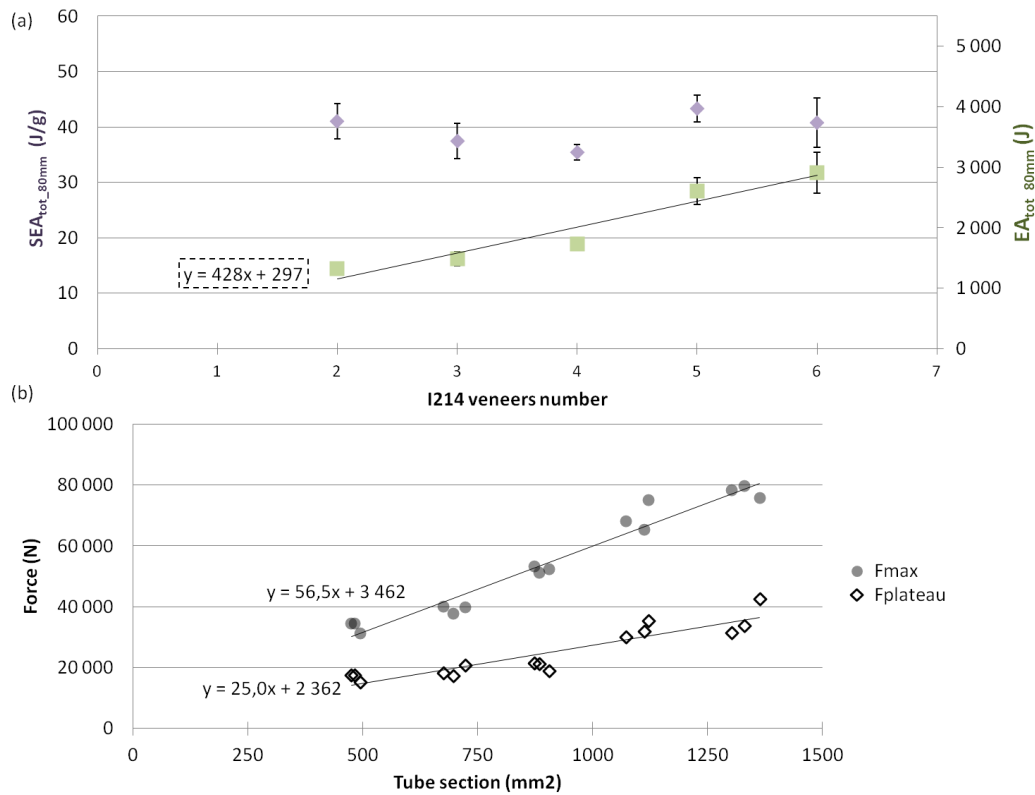


Fig. 11: Evolution of EA_{tot_80mm} and SEA_{tot_80mm} versus the number of I214 layers. (b) Maximum and plateau force versus tube sections for tubes with glass skins.

The increase in the energy absorbed for the three- and four-layer configuration was not significantly high compared to the increase in the mass of the sandwich and, therefore, the SEA decreased from 40.8 J / g on average to 37.5 then 35.4 J / g. The same observation was made for configurations with five and six poplar layers, where the absorbed energy gained thanks to the additional poplar layers was insufficient to give a gain in SEA. The differences in SEA between the configurations having three and four layers are difficult to explain. As with CFRP tubes, it was observed on several tubes that the failure front could have a different number of I214 folds splayed towards the inside of the tube on the same plane. As the energy absorbed increases linearly with the number of I214 folds, it can be represented by: $EA_{tot_80mm} = 428 \times number\ layer_{I214} + 297$, where 428 J is the contribution of each I214 layer and 297 J the contribution of the glass fibre skins. As with carbon fibre skins, the failure

mechanisms were more efficient in the loading phase than in the plateau phase. The average crushing stress of an I214 ply surrounded by glass fibres was 25 MPa.

3.3. Comparison between static and dynamic crushes

3.3.1. Tubes with carbon skins.

In this part, the static and dynamic performances obtained on the configuration [2CFRP-[0_N]-2CFRP]_{2≤N≤6} are compared. But, first, the crushes of CFRP monolithic tubes with 4 carbon layers (Fig. 12) are studied in order to see the influence of the static and dynamic behaviour of wood coupled to carbon fibres. The crushing of the CFRP tubes was carried out at the same speed as the crushing of the sandwich tubes (8.8 m / s).

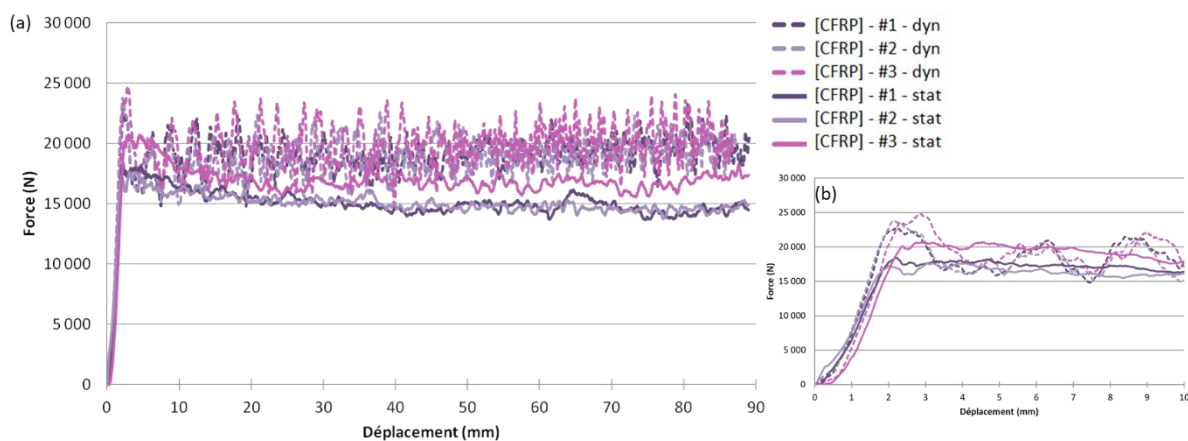


Fig. 12: (a) Static and dynamic crushing of tubes with carbon skins, (b) Zoom on initiation.

Again, the three crushing phases were found in both statics and dynamics. The oscillations were much greater in dynamics than in statics, even though no filtering was applied. The performances (Tab. 4) showed a slightly higher peak load in dynamic than in static configuration but the CFE was not degraded because the plateau also increased in dynamic tests and gave a CFE of 0.82 in dynamic and 0.80 in static.

		Mass g	Thickness mm	F _{max} N	L _{plateau} mm	F _{plateau} N	CFE	EA _{tot_80mm} J	SEA _{tot_80mm} J/g
Static test	CFRP - I	27.7	0.97	18 434	79.2	14 942	0.81	1 203	64.6
	CFRP - II	27.9	0.97	17 603	80.7	14 947	0.85	1 196	63.7
	CFRP - III	27.6	0.97	20 729	79.3	16 821	0.81	1 340	71.8
	Average	27.7	0.97	18 922	79.7	15 570	0.82	1 247	66.7

	Standard deviation	0.2	0.00	1 619	0.8	1 083	0.02	81	4.5
Dynamic test	CFRP - I	27.5	0.97	23 232	85.6	19 060	0.82	1 499	80.9
	CFRP - II	27.7	0.99	23 783	82.9	18 897	0.79	1 491	79.8
	CFRP - III	27.7	0.97	24 780	84.0	19 789	0.80	1 557	83.2
	Average	27.6	0.98	23 932	84.2	19 249	0.80	1 516	81.3
	Standard deviation	0.1	0.01	785	1.3	475	0.01	36	1.7

Tab. 4: Results for static and dynamic crush of monolithic [CFRP] tubes.

The gain in specific energy absorption in dynamic tests was 14.6 J/g. The dynamic performance of carbon tubes was thus higher than in the static situation. The failure mode between statics and dynamics was also different. In static conditions, the damage was caused by the progressive formation of petals via splaying (Fig. 13). In dynamics, the post-mortem observation did not reveal whether the numerous debris generated during the test were created by splaying or by fragmentation. Viewing the videos obtained by the fast cameras did not decide this point either. The [CFRP] tubes were therefore cut in half in order to observe the failure front under the microscope (Fig. 14).

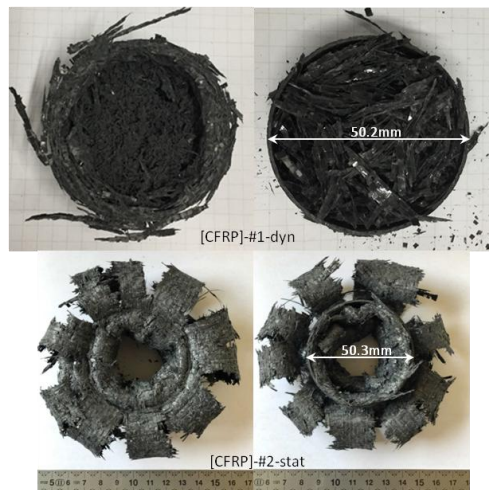


Fig. 13: Static and dynamic [CFRP] post-mortem failure pattern (chamfered side of the tube: photo on left; top of the tube: photo on right)

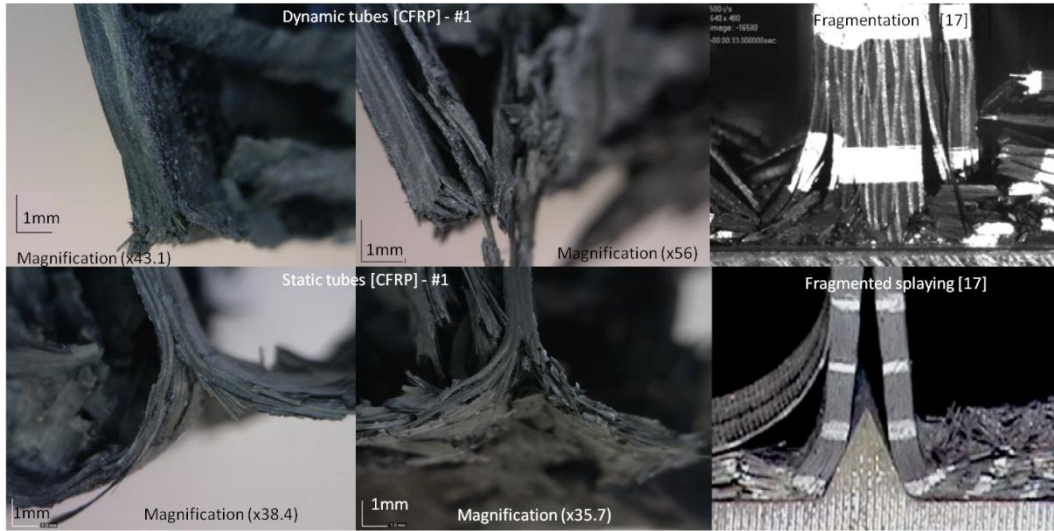


Fig. 14: Comparison of static and dynamic failure patterns of [CFRP] tube via microscopic observation (Right from [31]).

The static front shows splaying accompanied by failures in the laminate similar to the failure mode obtained by Guillon and called fragmented splaying [31]. Concerning the dynamic failure front, the absence of central cracking indicates more a classical dynamic failure mode of fragmentation which can be explained by a more fragile behaviour of the carbon fibres or the matrix with the increase in the strain rate.

Now, the results for the sandwich tubes are discussed. The averaged $[2\text{CFRP}-[0_N]-2\text{CFRP}]_{2 \leq N \leq 6}$ curves are superimposed in Fig. 15.

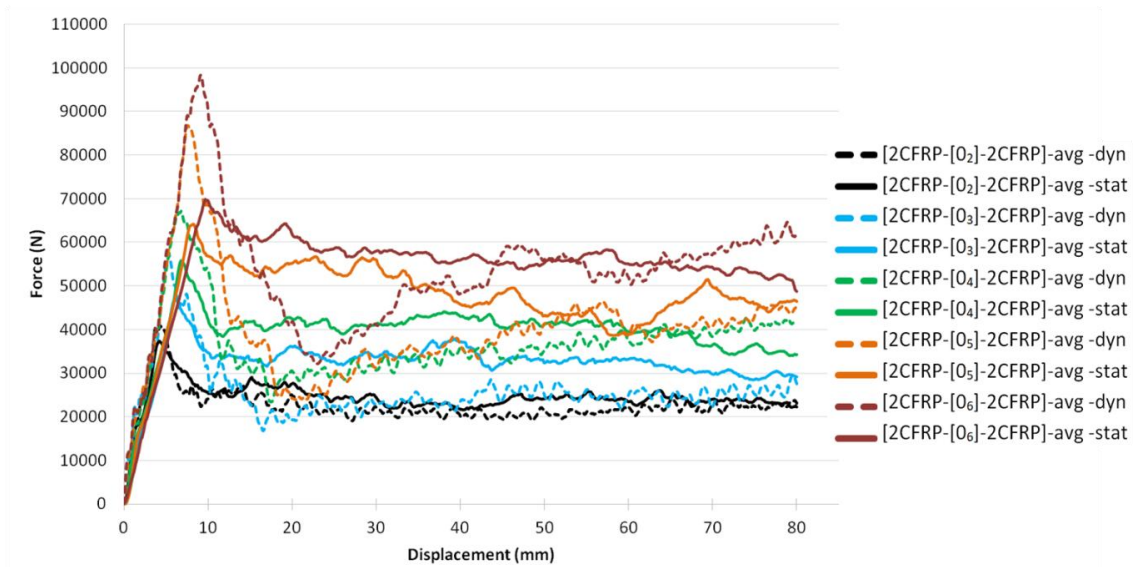


Fig. 15: Mean dynamic and static force-displacement curves of sandwich tubes $[2\text{CFRP}-[0_n]-2\text{CFRP}]_{2 \leq n \leq 6}$

The peak load is much higher in dynamic than in static (98,466 N for six poplar layers in dynamic versus 70,074 N in static, for example). An examination of the crushing plateau shows that the dynamic levels are lower than the static in each configuration. Thus, the dynamic CFE (varying from 0.41 to 0.57) is degraded in comparison to the static (varying from 0.63 to 0.85). The second observation concerns the transition phase, which differs from dynamic to static. In fact, in dynamics, after the peak load, the force decreases during about ten millimetres of crushing and then reaches the plateau. The transition phase is thus longer in dynamics than in statics. In addition, in dynamics, the plateau increases as the crushing progresses, more particularly for the configurations having four, five or six poplar layers. This is probably in connection with the compaction of the debris inside the tube, which results in a larger volume of debris for globally the same overall dimensions of the tube. In both statics and dynamics, the energy absorbed increased linearly with the number of I214 layers (Fig. 17). The equation shows that the contribution of a wood ply is slightly greater in dynamics (606 J) than in statics (576 J). The y-intercept provides information on how CFRP skins behave. They can be seen to absorb less energy dynamics (412 J) than in statics (851 J). In dynamic tests, the CFRP tubes alone absorbed an energy of 1516 J, showing that they work better on their own than as the skin of sandwich tubes. However, CFRP skins stabilized the I214 layers oriented at 0° thus improving the crash behaviour of the sandwich. The average value as a function of the number of I214 layers of the dynamic SEA is also more dispersed than the static SEA.

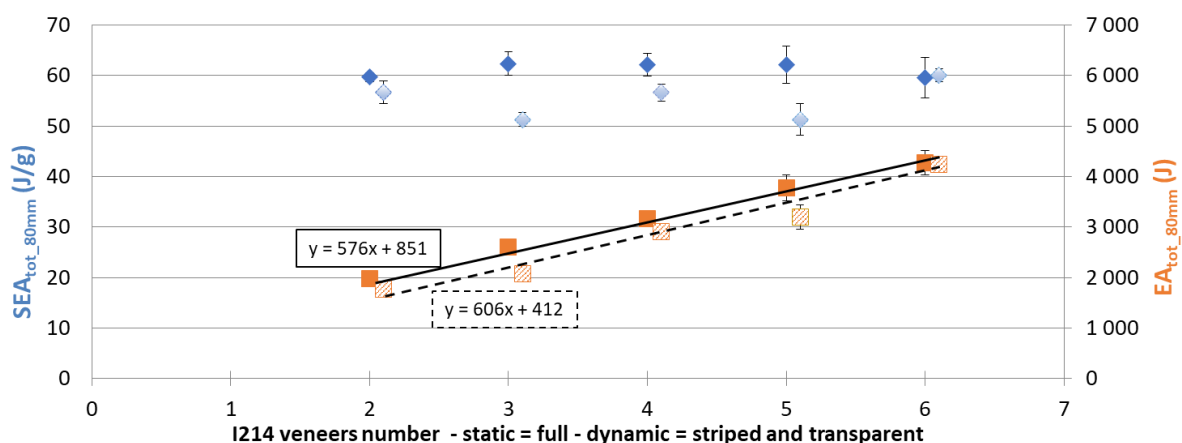
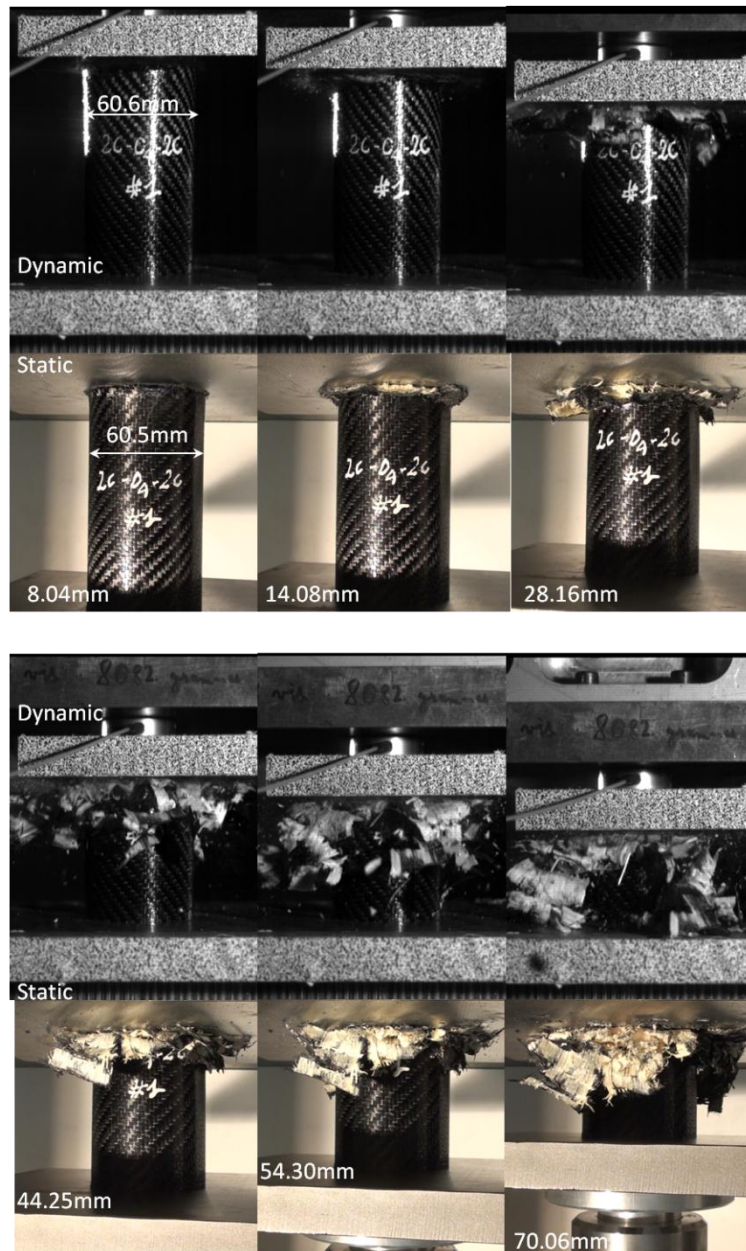


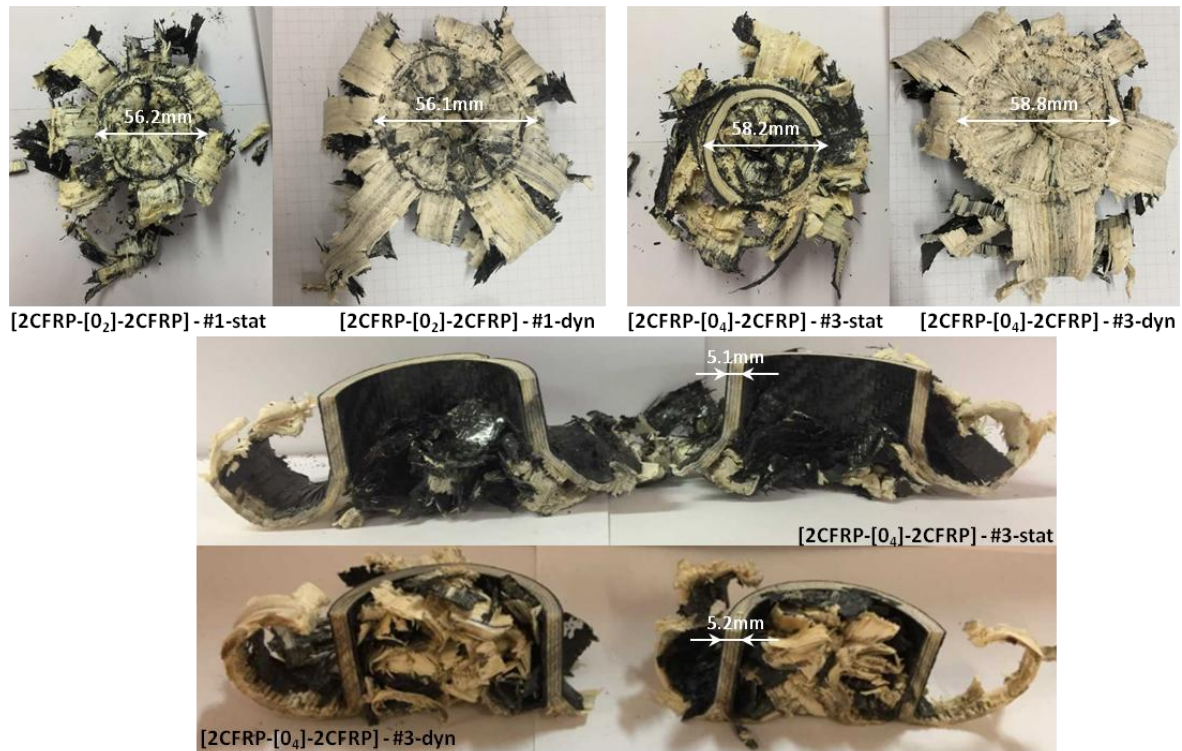
Fig. 16: Evolution of EA_{tot_80mm} and SEA_{tot_80mm} according to the number of I214 plies in static and dynamic for tubes with carbon skins.

Whether CFE, absorbed energy or SEA is considered, the dynamic performance of these sandwich tubes is slightly lower than their static performance. The average crushing stress with carbon fibre skins is almost identical between the static (37.2 MPa) and dynamic (34.9 MPa) regimes. A comparison of the static and dynamic failure modes shows that the overall failure is similar: splaying with the formation of petals (Fig. 18 and Fig. 19). However, certain phenomena, such as local buckling, are no longer present in the dynamic failure mode. Finally, it should also be noted that the compaction of the debris inside the tube is greater in dynamics (Fig. 19).



283
284

Fig. 17: Static and dynamic comparison of the failure mode of the tube [2CFRP-[0₄]-2CFRP]-#1 at iso-displacement (the static images have been turned).



285
286

Fig. 18: Static and dynamic comparison of post-mortem failure patterns for tubes with carbon skins.

287
288

3.3.2 Tubes with glass skins

289

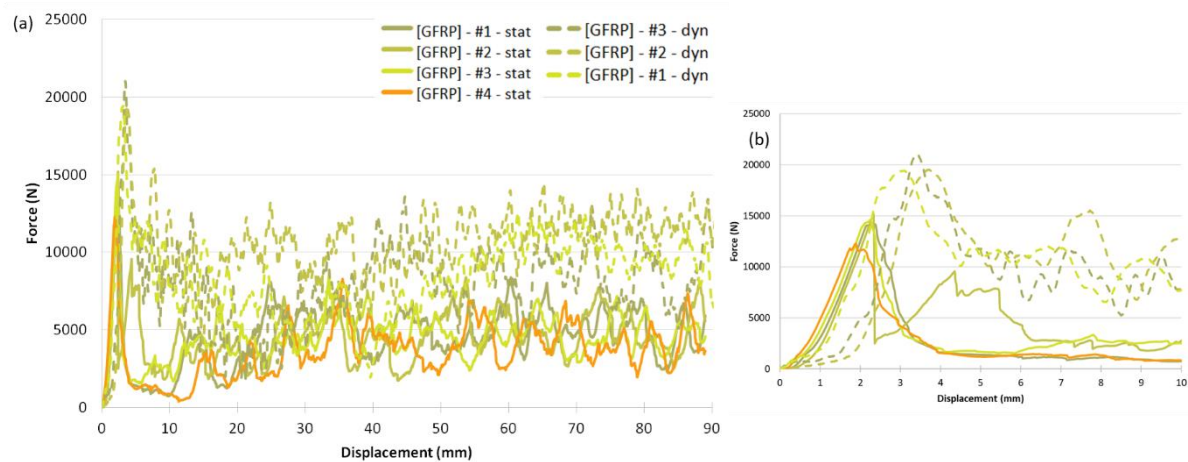
The static and dynamic performance of the sandwiches [2GFRP-[0_N]-2GFRP]_{2≤N≤6} were compared.

290

First, the crushes of monolithic GFRP tubes with four GFRP layers (Fig. 12) were studied to investigate

291

the influence of the static and dynamic behaviour of wood coupled with carbon fibres.



292
293

Fig. 19: (a) Static and dynamic crushing of monolithic glass tubes (b) Focus on initiation

Once again, the three classical phases were found in static and dynamic. On the overall reading of the crushing curves, an improvement in the energy absorption capacities of the dynamic glass fibre tubes was observed. The average plateau force was almost doubled, resulting in the doubling of the energy absorbed and the SEA (Tab. 5).

		Mass g	Thickness mm	F _{max} N	L _{plateau} mm	F _{plateau} N	CFE /	EA _{tot_80mm} J	SEA _{tot_80mm} J/g
Static tests	[GFRP] - #1	24.2	0.65	14 179	76.0	4 860	0.34	369	22.6
	[GFRP] - #2	24.3	0.68	15 178	83.3	4 476	0.29	363	22.2
	[GFRP] - #3	23.7	0.67	14 617	77.5	4 674	0.32	359	22.5
	[GFRP] - #4	23.7	0.67	12 275	74.7	3 985	0.32	291	18.3
	Average	24.0	0.67	14 062	77.9	4 499	0.32	364	21.4
	Standard deviation	0.3	0.01	1 260	3.8	377	0.02	37	2.1
Dynamic tests	[GFRP] - #1	24.8	0.70	19 430	88.4	8 230	0.42	656	39.6
	[GFRP] - #2	25.0	0.75	19 525	87.1	10 329	0.53	793	47.5
	[GFRP] - #3	25.1	0.72	21 015	85.4	7 923	0.38	632	37.8
	Average	25.0	0.72	19 990	87.0	8 827	0.44	694	41.6
	Standard deviation	0.1	0.03	889	1.6	1 310	0.08	87	5.2

Tab. 5: Static and dynamic [GFRP] tube crush results.

The increase in absorbed energy and SEA can be explained by a difference in failure mode between static and dynamic. During the static crush, large pieces of debris were created (of the order of a few centimetres) accompanied by instability of the walls of the tube, leading to very little energy absorption. In dynamics, the size of debris was much smaller (dust was visible on high speed camera images) although some macroscopic debris was created (Fig. 21). Post-mortem observation of the dynamic tubes showed the occasional presence of petals that were created by local splaying or via full-thickness bending.



Fig. 20: Static and dynamic [GFRP] tube post-mortem patterns (chamfered side of the tube: photo on the left; top of the tube: photo on the right)

Observation of the thickness of a half-tube [GFRP] under a microscope indicated the absence of a longitudinal crack (synonymous with splaying) and showed that the creation of debris took place by bending causing intralaminar cracks (Fig. 22). Therefore the dynamic and static failure mode was fragmentation, with smaller debris in dynamics, which dissipated more energy.

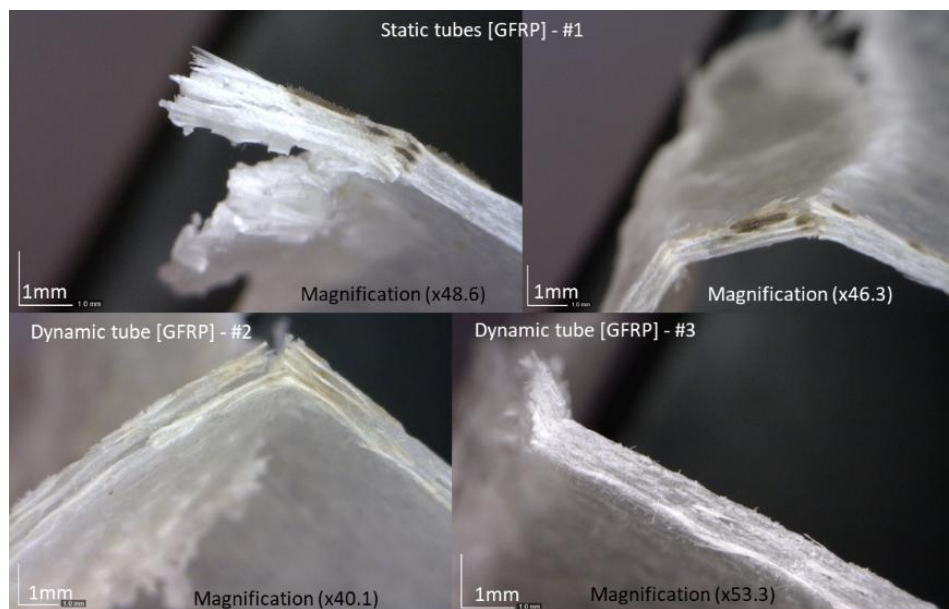


Fig. 21: Comparison of static and dynamic failure patterns of [GFRP] tubes via microscopic observation.

Now, the results for the sandwich tubes are discussed. The averaged curves of static and dynamic test results versus the number of poplar layers have been superimposed in Fig. 23.

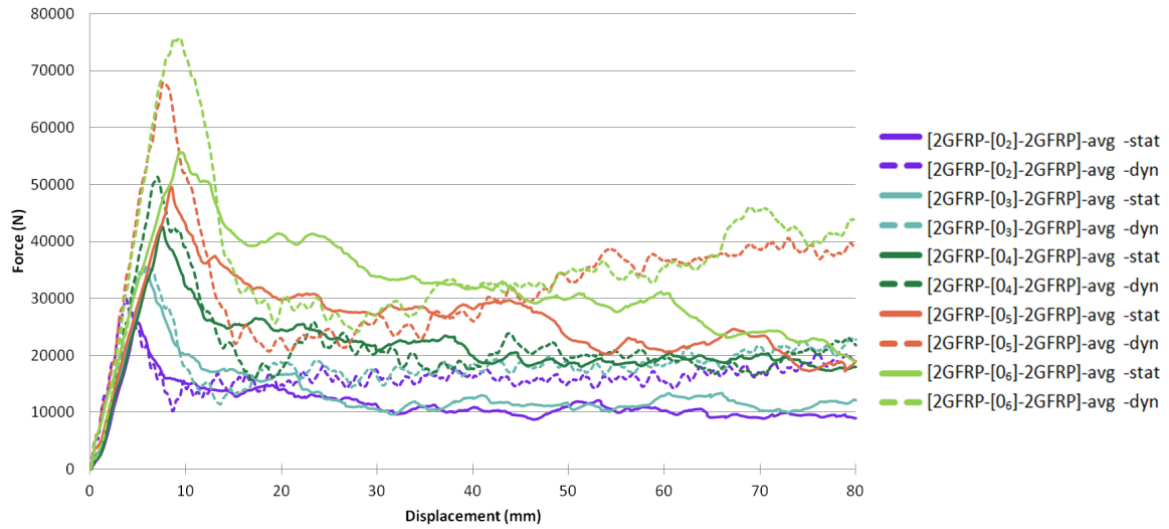


Fig. 22: Averaged dynamic and static force-displacement curves of tubes $[2\text{GFRP}-[0_n]-2\text{GFRP}]_{2 \leq n \leq 6}$

A first observation concerns the change of the apparent slope between static and dynamic conditions. In dynamics, the slope is greater than in static (Fig. 23) for all configurations. As the pseudo-linear slope of the glass fibre tubes also changed between the static and dynamic regimes, this behaviour can be attributed to the I214 poplar, the glass fibres or the coupling of the two materials. The second observation is that the performance of sandwich tubes with glass fibre skins was improved in dynamics (Fig.24).

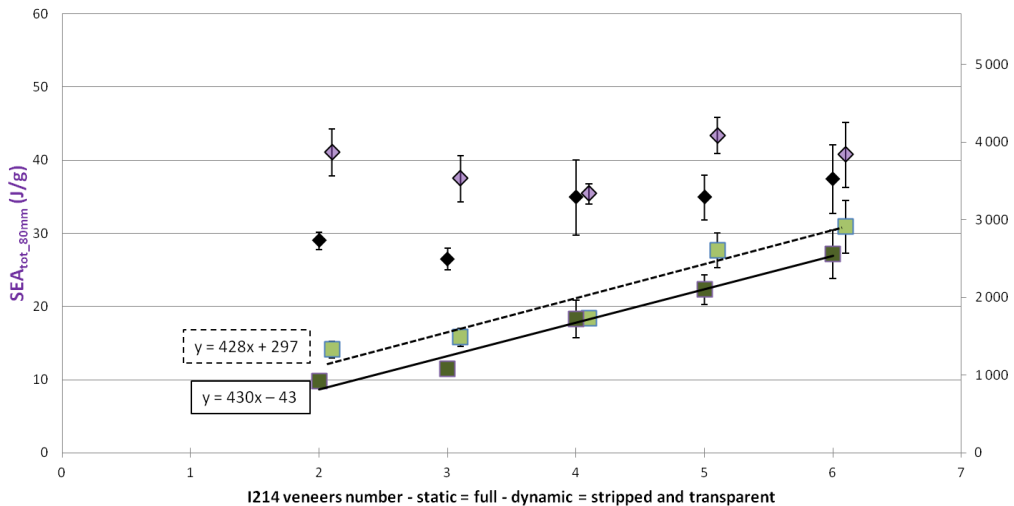


Fig. 24: Evolution of $EA_{tot,80mm}$ and $SEA_{tot,80mm}$ according to the number of I214 plies in static and dynamic for tubes with glass skins.

The slope modelling the absorbed energy presented an identical director coefficient in dynamics and statics. In addition, the average crushing stress of an I214 ply surrounded by glass fibres changed very little or not at all between the static (24.3 MPa) and the dynamic (25 MPa) tests. The comparison of

static and dynamic post-mortem failure patterns showed a fairly similar mode of failure with mainly the formation of petals after splaying (Fig. 25). However, the local buckling observed in statics disappeared in dynamics and the compaction of debris was much greater in dynamics than in statics, as for tubes with carbon skins (Fig. 26). The debonding of interior fibreglass skins was also much greater in static than in dynamic.

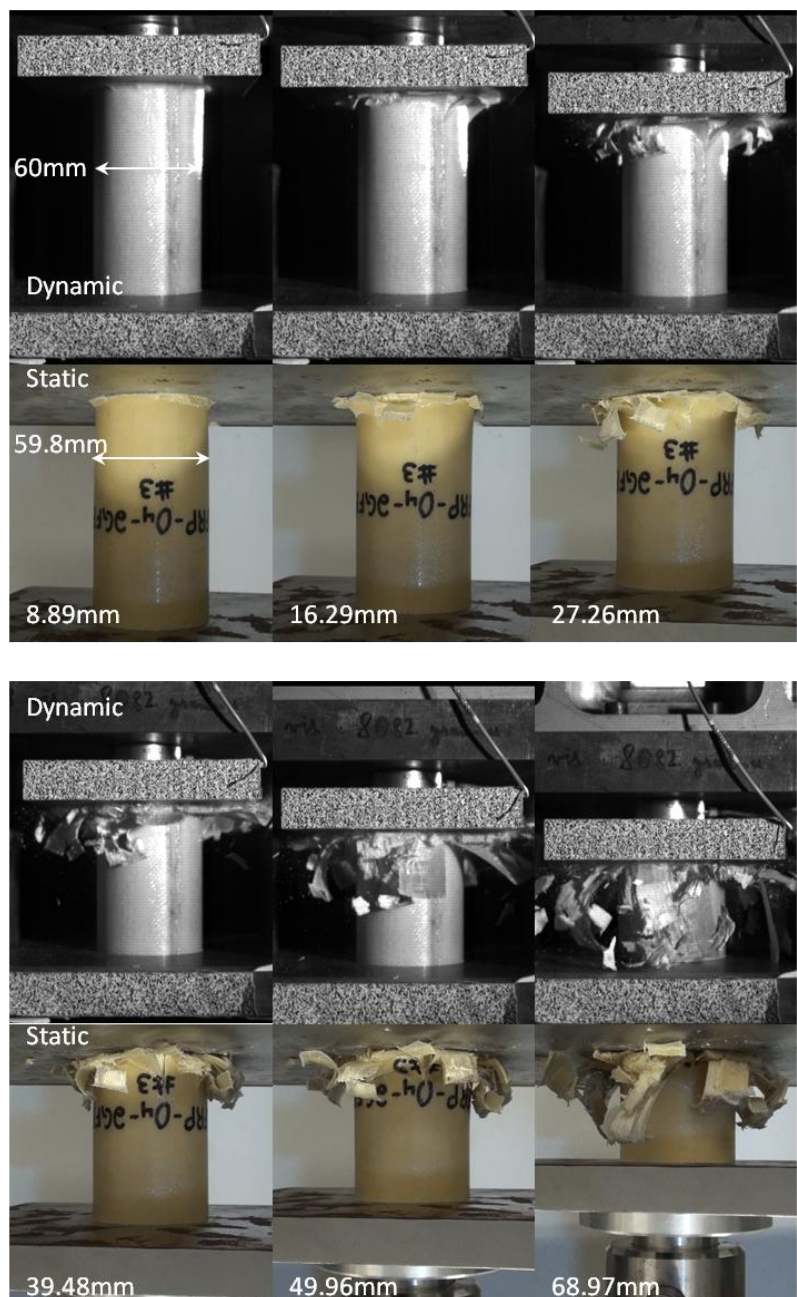


Fig. 25: Static and dynamic comparison of the failure mode of the tube [2GFRP-[0₄]-2GFRP]-#3 at iso-displacement (the static images have been turned).

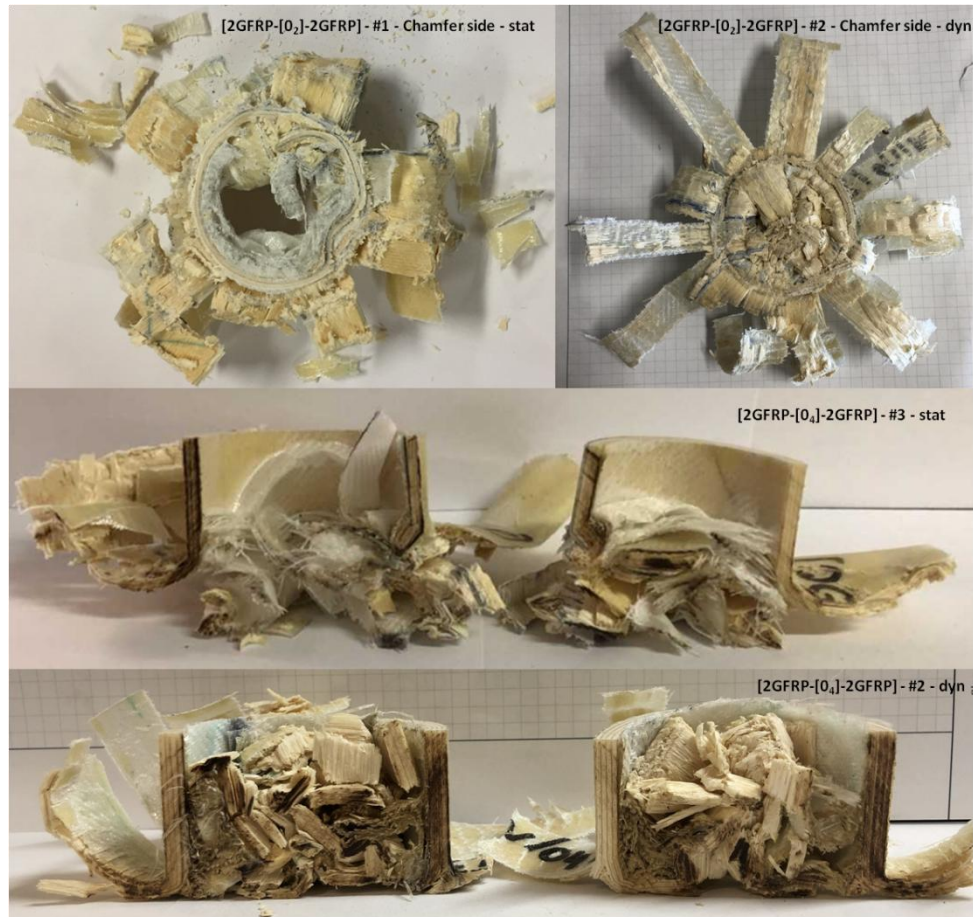


Fig. 26: Static and dynamic comparison of the post-mortem failure pattern for tubes with glass skins.

3.4. Coupling gains between wood core and composite skins

To assess the coupling effects, the approach adopted was as follows. The crushed tubes [CFRP] and [GFRP] shown in Tab. 4 and Tab. 5 correspond to the equivalent of the outer and inner skins of sandwich tubes [2CFRP-[0₆]-2CFRP] and [2GFRP-[0₆]-2GFRP]. For the equivalent of these sandwich tubes using wood core alone, it was not possible to consider the poplar-only tubes [0₆] (6 layers in the longitudinal direction) as, due to a very unstable mode of failure, the possible contribution of the wood to the energy absorption was very low and not significant [29]. So the most stable configuration, still with six layers of poplar but with only four plies in the longitudinal direction [90/0₄/90] was considered for the reference of the wood core. By cumulating the crushing of the tubes [CFRP] (or [GFRP]) and the equivalent of the core [90/0₄/90], and comparing them to the direct crushing of the tubes [2CFRP-[0₆]-2CFRP] (or [2GFRP-[0₆]-2GFRP]), the coupling effect was deduced.

3.4.1. Tubes with Carbon skins

The results are presented in Fig. 27 and Tab. 6 and the results obtained in static [30] are recalled. A gain of 41% can be noted for the strength of the plate, 35% for the energy absorbed and 40% for the SEA, showing the interest of merging these materials. However, the gain is slightly lower than in static conditions (Tab. 6). This slightly lower gain can be explained by the fact that the CFRP tube alone shows an improvement in its dynamic SEA (+ 14.6 J/g), while the sandwich tube with carbon fibre skins keeps an identical SEA (0.5 J/g difference).

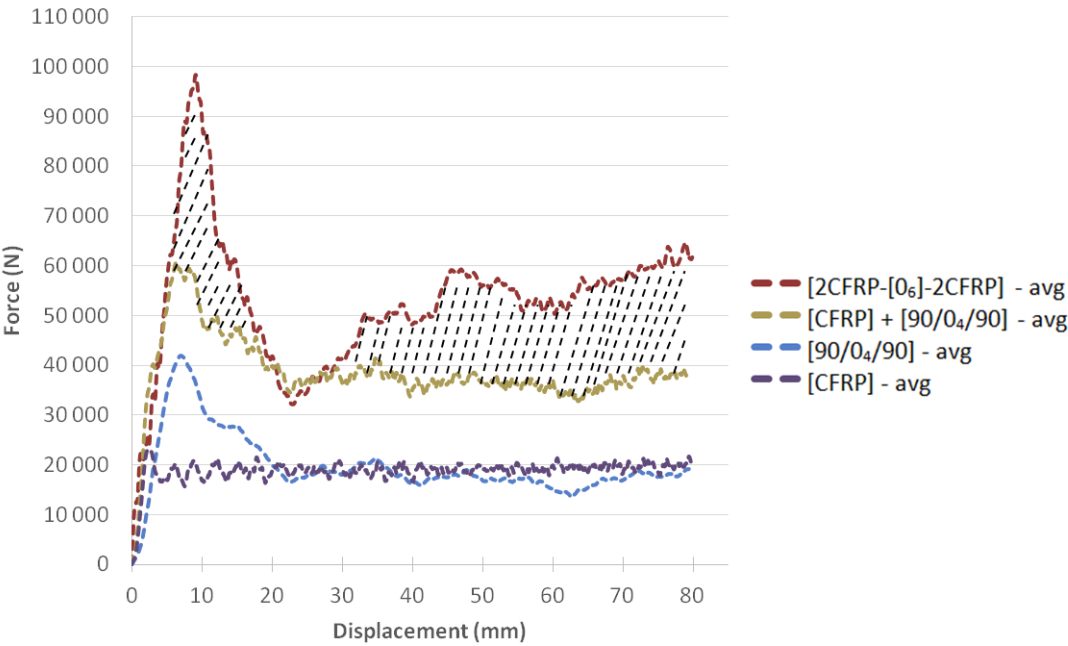


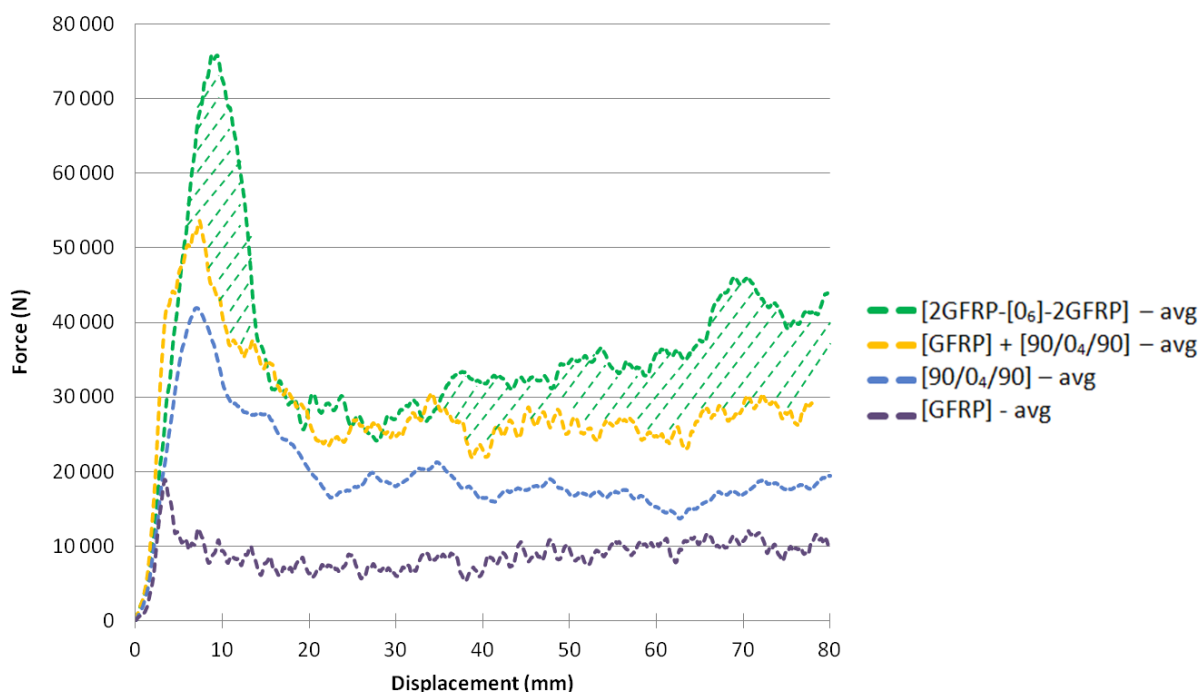
Fig. 27: Dynamic coupling for sandwich [2CFRP-[0₆]-2CFRP]

		F _{plateau} N	EA _{tot_80mm} J	Mass g	SEA _{tot_80mm} J/g
Static	[90/0 ₄ /90] – avg	21 019	1 632	76.6	30.6
	[CFRP] – avg	15 570	1 247	27.7	66.7
	[90/0 ₄ /90] + [CFRP] – avg	36 589	2 879	104.3	40.6
	[2CFRP-[0 ₆]-2CFRP] – avg	55 551	4 264	102.9	59.5
	Coupling gain	52%	48%		47%
Dynamic	[90/0 ₄ /90] – avg	17 940	1 618	72.8	31.5
	[CFRP] – avg	19 249	1 516	27.6	81.3
	[90/0 ₄ /90] + [CFRP] – avg	37 189	3 134	100.4	42.9
	[2CFRP-[0 ₆]-2CFRP] – avg	52 459	4 235	102.0	60.0
	Coupling gain	41%	35%		40%

Tab. 6: Gain obtained by coupling wood core and carbon skins.

366 3.4.1. Tubes with glass skins

367 The dynamic coupling for glass skins is shown in Fig. 28 and Tab 7.



368 Fig. 28: Dynamic coupling for sandwich [2GFRP-[0₆]-2GFRP]

369 The dynamic coupling allowed gains of 20% and 22% on the absorbed energy and the SEA, respectively (Tab. 7). The gain of the coupling in dynamics was slightly lower than that obtained in statics: the [GFRP] tube showed a gain in SEA of 20.2 J / g between the static and the dynamic tests, resulting in an energy difference of 330 J.

		F _{plateau} N	EA _{tot_80mm} J	Mass g	SEA _{tot_80mm} J/g
Static	[90/0 ₄ /90] - avg	21 019	1 632	76.6	30.6
	[GFRP] - avg	4 670	364	24.0	21.4
	[90/0 ₄ /90] + [GFRP] - avg	25 689	1 996	100.6	29.9
	[2GFRP-[0 ₆]-2GFRP] - avg	28 995	2 556	99.2	37.4
	Coupling gain	13%	28%		25%
Dynamic	[90/0 ₄ /90]-avg	17 940	1 618	72.8	31.5
	GFRP - avg	8 827	694	25.0	41.6
	[90/0 ₄ /90] + GFRP - avg	26 767	2 312	97.8	31.8
	[2GFRP-[0 ₆]-2GFRP] - avg	35 851	2 908	103.7	40.7
		25%	20%		22%

374 Tab. 7: Gain obtained by coupling wood core and glass skins.

375

3.5. Comparison of tubes with carbon and glass skins

Fig. 29 shows a superposition of the dynamic curves of the glass and carbon fibre sandwich tubes.

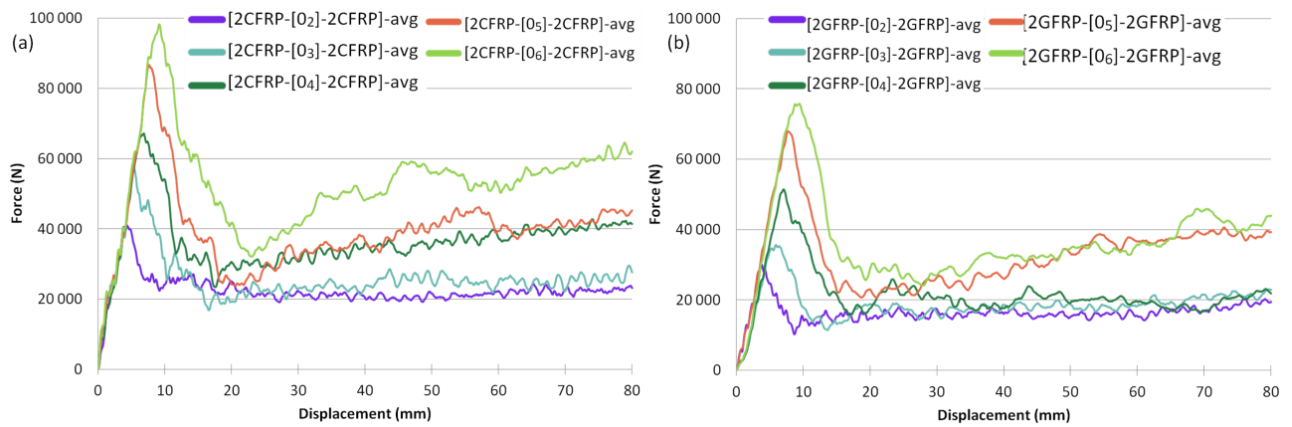


Fig. 29: Comparison of dynamic crushing of (a) CFRP and (b) GFRP skins.

The peak load on tubes with carbon fibre skins is higher than for those made of glass fibres. Average stress levels on carbon fibres are higher than those obtained with glass fibres. The energies absorbed and the SEA according to the types of skin and the number of I214 layers are compared in Fig. 30.

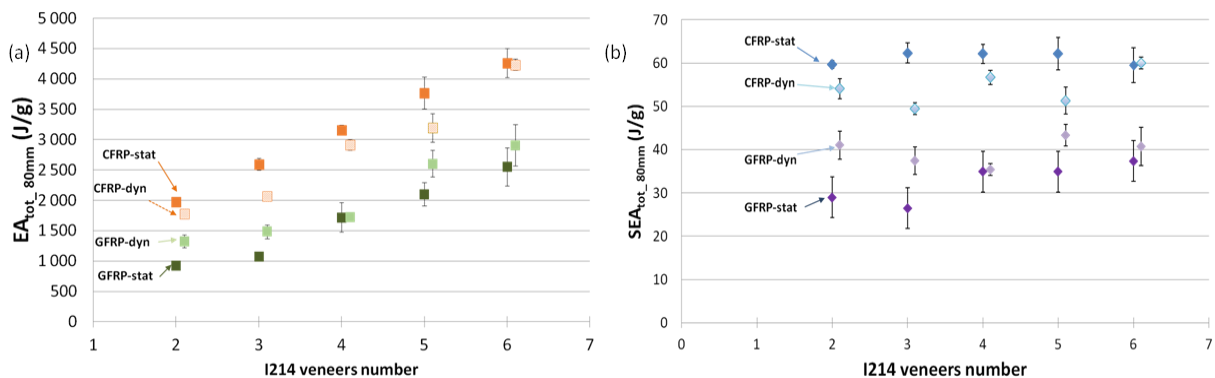


Fig. 30: Evolution of (a) $EA_{tot,80mm}$ (b) $SEA_{tot,80mm}$ according to the number of poplar layers, the nature of the skins, and static and dynamic conditions.

The energy absorbed, whether with carbon fibre or glass fibre skins, has an almost linear relationship with the number of I214 poplar veneers. The linear increase in absorbed energy does not lead to an increase in SEA, which can be considered almost constant. In static and for carbon fibre skins, the SEA oscillates around a value of 61.2 J / g and, in dynamics, around an average value of 54.3 J / g. With the fibreglass skins, in static mode and with the passage from 3 to 4 plies, a slight increase in the SEA is to be noted before it stagnates at a value of 35.7 J / g. Dynamically, glass fibre skins exhibit a more regular SEA oscillation around an average value of 39.5 J / g.

394

395 **4. Conclusions and perspectives**

396 Dynamic crushing tests of sandwich tubes with carbon fibre or glass - epoxy resin skins and poplar
397 veneer core were investigated experimentally in this study. The tests showed that:

398 - The dynamic crushing of sandwich tubes with carbon skins [2CFRP-[0_N]-2CFRP]_{2≤N≤6} gave
399 interesting energy absorption results: an average dynamic SEA of 54.3 J / g. As the energy
400 absorbed evolved linearly with the number of I214 layers employed, the dynamic SEA oscillated
401 between 49.4 and 60 J/g. The monolithic CFRP tube had an SEA of 81.3 J/g versus a
402 maximum of 60 J/g but the plateau force was 52,459 N for the sandwiches and 19,249 N for the
403 CFRP tubes alone. An increase in the initial pseudo-linear slope between statics and dynamics
404 was also observed. This can be attributed either to the carbon or to the wood or to the coupling
405 of the two, since these two materials also showed an increase in apparent modulus in
406 dynamics. The predominant failure mode in statics and dynamics was splaying. In dynamics,
407 the internal confinement of debris was more pronounced than in statics. The combined use of
408 poplar and carbon fibres allowed a gain on the SEA of the order of 40% in dynamics compared
409 to the sum of the two materials crushed independently.

410 - The dynamic crushing of sandwich tubes with glass skins [2GFRP-[0_N]-2GFRP]_{2≤N≤6} also
411 showed interesting energy absorption results. An average SEA of 39.3 J / g was obtained in
412 dynamic tests. The static and dynamic failure patterns of these tubes showed the formation of
413 petals induced by splaying. The internal containment of debris was more marked in dynamics
414 than in statics. The crushing of a monolithic glass fibre tube (of the same thickness as the skins)
415 showed a strong improvement in its dynamic energy absorption properties: its unstable crushing
416 in static generated large pieces of debris whereas the creation of fewer large and more
417 microscopic pieces in dynamic led to more dissipative properties, raising the SEA from 21.4 J /
418 g to 41.6 J / g. With the glass fibre skins in dynamics, the insertion of the I214 veneers as core
419 materials allowed an elevation of the crush plate for an equivalent SEA and also presented

interesting coupling of the two materials, with a gain of 20 % of energy absorbed and 22% on SEA. In the same way as with carbon fibre skins, the transition from static to dynamic produced a greater load peak and a pseudo-linear slope.

Globally, the dynamic behaviour of these sandwiches with a poplar core confirms the results obtained in statics and the significant contribution in terms of energy absorbed by the wood core. Indeed, when the number of poplar layers of the core increase from two to six, the absorbed energy is doubled. The SEA obtained for the configurations studied is comparable to those of other materials (Fig. 33) but minimizes the use of composites in favour of wood. Because poplar is a wood species with a relatively low density, and thus with some of the lowest intrinsic mechanical characteristics, work on various wood species is envisaged in order to study their crash aptitudes and compare their behaviour and performance with those of poplar I214.

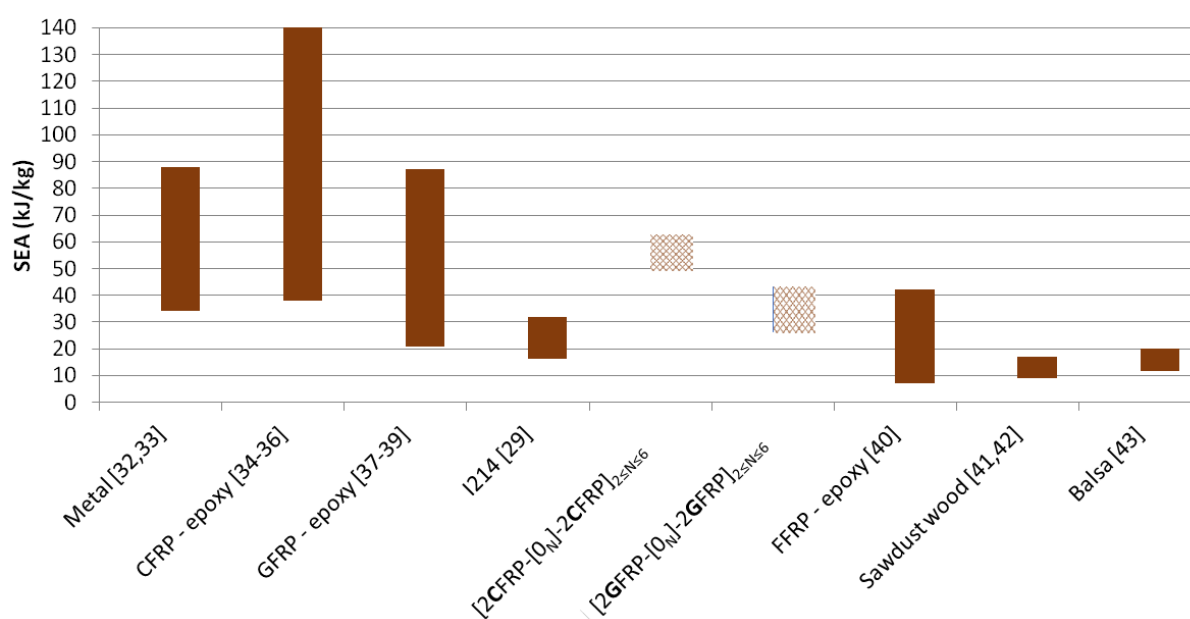


Fig. 23: SEA from of some materials ([29], [30]).

5. Acknowledgements

The authors thank the French Government for providing financial support (MESRI) and the Garnica company for providing I214 veneers for this study.

6. References

- [1] Forest Product Laboratory. Wood Handbook Wood as an Engineering Material. United States Department of Agriculture, Forest Service; 2010.
- [2] R. Bergman, M. Puettmann, A. Taylor, and K.E. Skog, "The Carbon Impacts of Wood Products," *For. Prod. J.* vol. 64, pp 220–31, 2014. <https://doi.org/10.13073/FPJ-D-14-00047>.
- [3] R. Asada, G. Cardellini, C. Mair-Bauernfeind, J. Wenger, V. Haas, D. Holzer, et al., "Effective bioeconomy? A MRIO-based socioeconomic and environmental impact assessment of generic sectoral innovations," *Technol. Forecast. Soc. Change.* Vol 153, n°119946, 2020;153:<https://doi.org/10.1016/j.techfore.2020.119946>.
- [4] B. Castanie, C. Bouvet, M. Ginot, "Review of composite sandwich structure in aeronautic applications," *Comp. Part. C Open Access*, Vol. 1, n° 100004, 2020. <https://doi.org/10.1016/j.jcomc.2020.100004>.
- [5] <https://www.robin-aircraft.com/> accessed 2021/07/09
- [6] <https://www.avionsmauboussin.fr/> accessed 2021/07/09
- [7] <https://aura-aero.com/> accessed 2021/07/09
- [8] D. Kohl, P. Link and S. Böhm, "Wood as a Technical Material for Structural Vehicle Components," *Procedia CIRP*, Vol. 40, pp 557–61, 2016. <https://doi.org/10.1016/j.procir.2016.01.133>.
- [9] Consortium WoodC.A.R. <https://www.woodcar.eu/index.html>. accessed 2021/07/09
- [10] J. Susainathan, F. Eyma, E. De Luycker, A. Cantarel and B. Castanie, "Manufacturing and quasi-static bending behavior of wood-based sandwich structures," *Comp. Struct.*, Vol. 182, pp 487–504, 2017. <https://doi.org/10.1016/j.compstruct.2017.09.034>.
- [11] J. Smardzewski and K.W. Wojciechowski, "Response of wood-based sandwich beams with three-dimensional lattice core," *Comp. Struct.*, Vol. 2016, pp 340–49, 2019. <https://doi.org/10.1016/j.compstruct.2019.03.009>.
- [12] S.W. Kavermann and D. Bhattacharyya, "Experimental investigation of the static behaviour of a corrugated plywood sandwich core," *Comp. Struct.* Vol. 207, pp 836–44, 2019. <https://doi.org/10.1016/j.compstruct.2018.09.094>.
- [13] J. Liu , T. Zhang, W. Jiang Wand J. Liu, "Mechanical response of a novel composite Y-frame core sandwich panel under shear loading" *Comp. Struct.*, Vol. 224, n° 111064, 2019. <https://doi.org/10.1016/j.compstruct.2019.111064>.
- [14] J. Smardzewski, "Experimental and numerical analysis of wooden sandwich panels with an auxetic core and oval cells," *Mat. Des.*, Vol. 183, n° 108159, 2019. <https://doi.org/10.1016/j.matdes.2019.108159>.
- [15] X. Wang, X. Shi, Q. Meng, Y. Hu and L. Wang, "Bending behaviors of three grid sandwich structures with wood facing and jute fabrics/epoxy composites cores," *Comp. Struct.*, Vol. 252, n°112666, 2020. <https://doi.org/10.1016/j.compstruct.2020.112666>.

- [16] F. Neveu, B. Castanié and P. Olivier, "The GAP methodology: a new way to design composite structures," *Materials & Design*, Vol. 172, n° 107755, 2019. <https://doi.org/10.1016/j.matdes.2019.107755>
- [17] C. Atas and C. Sevim, "On the impact response of sandwich composites with cores of balsa wood and PVC foam," *Comp. Struct.*, Vol.93, pp 40–48, 2010. <https://doi.org/10.1016/j.compstruct.2010.06.018>.
- [18] J. Susainathan, F. Eyma, E. De Luycker, A. Cantarel and B Castanié, "Experimental investigation of impact behavior of wood-based sandwich structures," *Comp. Part A, Appl. Sci. Manuf.*, Vol. 109, pp 10-19, 2018. . <https://doi.org/10.1016/j.compositesa.2018.02.029>.
- [19] J. Susainathan, F. Eyma, E. De Luycker, A. Cantarel and B Castanié, "Numerical modeling of impact on wood-based sandwich structures", *Mech. Adv. Mat. Struct.*, Vol. 27, pp 1583–98, 2020. <https://doi.org/10.1080/15376494.2018.1519619>.
- [20] T.K. Demircioğlu, F. Balıkoğlu, O. İnal, N. Arslan, I. Ay and A. Ataş, " Experimental investigation on low-velocity impact response of wood skinned sandwich composites with different core configurations," *Mat. Today. Com.*, Vol. 17, pp 31–9, 2018. <https://doi.org/10.1016/j.mtcomm.2018.08.003>.
- [21] J. Smardzewski, "Wooden sandwich panels with prismatic core – Energy absorbing capabilities." *Comp. Struct.*, Vol. 230, n° 111535, 2019. <https://doi.org/10.1016/j.compstruct.2019.111535>.
- [22] G. Palomba, G. Epasto and V. Crupi, "Lightweight sandwich structures for marine applications: a review", *Mechanics of Advanced Materials and Structures*, on line, <https://doi.org/10.1080/15376494.2021.1941448>
- [23] W. Johnson, "Historical and present-day references concerning impact on wood," *Int. J. Impact. Eng.*, Vol. 4, pp 161–74, 1986. [https://doi.org/10.1016/0734-743X\(86\)90003-5](https://doi.org/10.1016/0734-743X(86)90003-5).
- [24] J. Susainathan, F. Eyma, E. De Luycker, A. Cantarel, C. Bouvet and B Castanié, "Experimental investigation of compression and compression after impact of wood-based sandwich structures", *Comp. Struct.*, Vol. 220, pp 236–49, 2019. <https://doi.org/10.1016/j.compstruct.2019.03.095>.
- [25] B. Castanié, J. J. Barrau, J. P. Jaouen, and S. Rivallant, "Combined shear/compression structural testing of asymmetric sandwich structures," *Exp. Mech.*, vol. 44, no. 5, pp. 461–472, 2004. DOI:10.1007/BF02427957.
- [26] F. Balıkoğlu T.K. Demircioğlu, O. İnal, N. Arslan and A. Ataş, "Compression after low velocity impact tests of marine sandwich composites: Effect of intermediate wooden layers," *Comp. Struct.*, Vol. 183, pp 636–42, 2018. <https://doi.org/10.1016/j.compstruct.2017.08.003>.
- [27] M. Neumann. *Investigation of the Behaviour of Shock-Absorbing Structural Parts of Transport Casks Holding Radioactive Substances in Terms of Design Testing and Risk Analysis*. Bergische Universität Wuppertal, 2009.
- [28] N. Butler, "Computer modelling of wood-filled impact limiters" *Nucl. Eng. Des.*, Vol. 150, pp 417–24, 1994. [https://doi.org/10.1016/0029-5493\(94\)90161-9](https://doi.org/10.1016/0029-5493(94)90161-9).

- [29] R. Guélou, F. Eyma, A. Cantarel, S. Rivallant, B. Castanié, "Crashworthiness of poplar wood veneer tubes", *Int. J. Impact. Eng.*, Vol. 147, n° 103738, 2021.
<https://doi.org/10.1016/j.ijimpeng.2020.103738>.
- [30] R. Guélou, F. Eyma, A. Cantarel, S. Rivallant, B. Castanié, "Static crushing of wood based sandwich composite tubes," *Comp. Struct.*, Vol. 273, n° 114317, 2021.
<https://doi.org/10.1016/j.compstruct.2021.114317>.
- [31] D. Guillon, « Etude des mécanismes d'absorption d'énergie lors de l'écrasement progressif de structures composites à base de fibre de carbone », PhD Thesis. Institut Supérieur de l'Aéronautique et de l'Espace, ISAE, Ecole doctorale : Mécanique, énergétique, génie civil et procédés, 2008.